minerals

MDPI

Article

Neodymium-Rich Monazite of the Lemhi Pass District, Idaho and Montana: Chemistry and Geochronology †

Virginia S. Gillerman [1,*], Michael J. Jercinovic [2] and Mark D. Schmitz [3]

[1] Idaho Geological Survey, Boise, ID 83702, USA
[2] Department of Earth, Geographic, and Climate Sciences, University of Massachusetts-Amherst, Amherst, MA 01003, USA; mjercino@umass.edu
[3] Department of Geosciences, Boise State University, Boise, ID 83725, USA; markschmitz@boisestate.edu
* Correspondence: vgillerm@uidaho.edu; Tel.: +1-208-332-4420
† This article is an expanded version of a talk which was presented at the Society for Geology Applied to Mineral Deposits (SGA) 2025 Meeting in Golden, CO, USA, 3–7 August 2025.

Abstract

Thorium-rare earth-iron oxide deposits of the Lemhi Pass district, Idaho and Montana, are enriched in the middle rare earth elements (REE), and particularly neodymium (Nd). Overall, thorium (Th) and total rare earth oxide (TREO) grades of the deposits are sub equal at 0.4 wt. % but locally exceed 1 wt. % TREO. Nd-monazite, the major REE phase (35 wt. % Nd_2O_3) occurs in hydrothermal Th-REE mineralized quartz veins and biotite-rich shear zones of enigmatic origin. Hosted in Mesoproterozoic metasedimentary rocks, the deposits are modest in size but present over a large area with no obvious source pluton exposed. This paper documents the geochemistry of the monazite and provides the first geochronological data to constrain its origin. Elemental mapping and U-Th-total Pb EPMA dating of the monazite and thorite document a Paleozoic age for mineralization centered in the Late Devonian at approximately 355 Ma ± 20 Ma. A second period of volumetrically minor Th and REE remobilization is dated as Mesozoic (ca. 100 Ma). For context, a reactivated passive continental margin was present during the Devonian in eastern Idaho, while the Mesozoic was a time of major accretionary tectonics and arc magmatism further west. Nd and Pb isotopic data require a significant interaction of the fluids with an ancient crustal component represented by regional Mesoproterozoic metasedimentary rocks and granitoids. A source–transport–deposition model is hypothesized with metasomatic fractionation and enrichment of Nd during regional hydrothermal circulation. The aqueous fluids were hot, oxidizing, and likely saline, but the exact source of the Th and REEs and the mechanism of enrichment remains problematic. Additional analytical work and increased knowledge of the regional and district geology will improve this unconventional hypothesis for formation of Lemhi Pass' unusual Nd-rich Th-REE-Fe mineralization.

Keywords: rare earths; neodymium; Idaho; monazite; geochronology; thorium

check for updates

Academic Editor: Bernhard Schulz

Received: 17 June 2025
Revised: 24 October 2025
Accepted: 27 October 2025
Published: 31 October 2025

Citation: Gillerman, V.S.; Jercinovic, M.J.; Schmitz, M.D. Neodymium-Rich Monazite of the Lemhi Pass District, Idaho and Montana: Chemistry and Geochronology. *Minerals* **2025**, *15*, 1156. https://doi.org/10.3390/min15111156

Copyright: © 2025 by the authors. Licensee MDPI, Basel, Switzerland. This article is an open access article distributed under the terms and conditions of the Creative Commons Attribution (CC BY) license (https://creativecommons.org/licenses/by/4.0/).

1. Introduction

The Lemhi Pass district is located along the Continental Divide between Idaho and Montana in the northern Rocky Mountains of the USA (Figure 1). The district is most notable in two respects. Historically, Lemhi Pass was where the Lewis and Clark Expedition first crossed the Divide in August 1805 on their quest for a path to the Pacific Ocean. Geologically, the district is host for over 200 thorium-rare earth veins within an approximately 140 sq. km area of the central Beaverhead Range. Unusually, neodymium (Nd) is a

dominant rare earth element (REE) in the veins, as first observed by early researchers and government geologists [1–3] and later substantiated with modern analytical methods. The main rare earth mineral at Lemhi Pass is monazite.

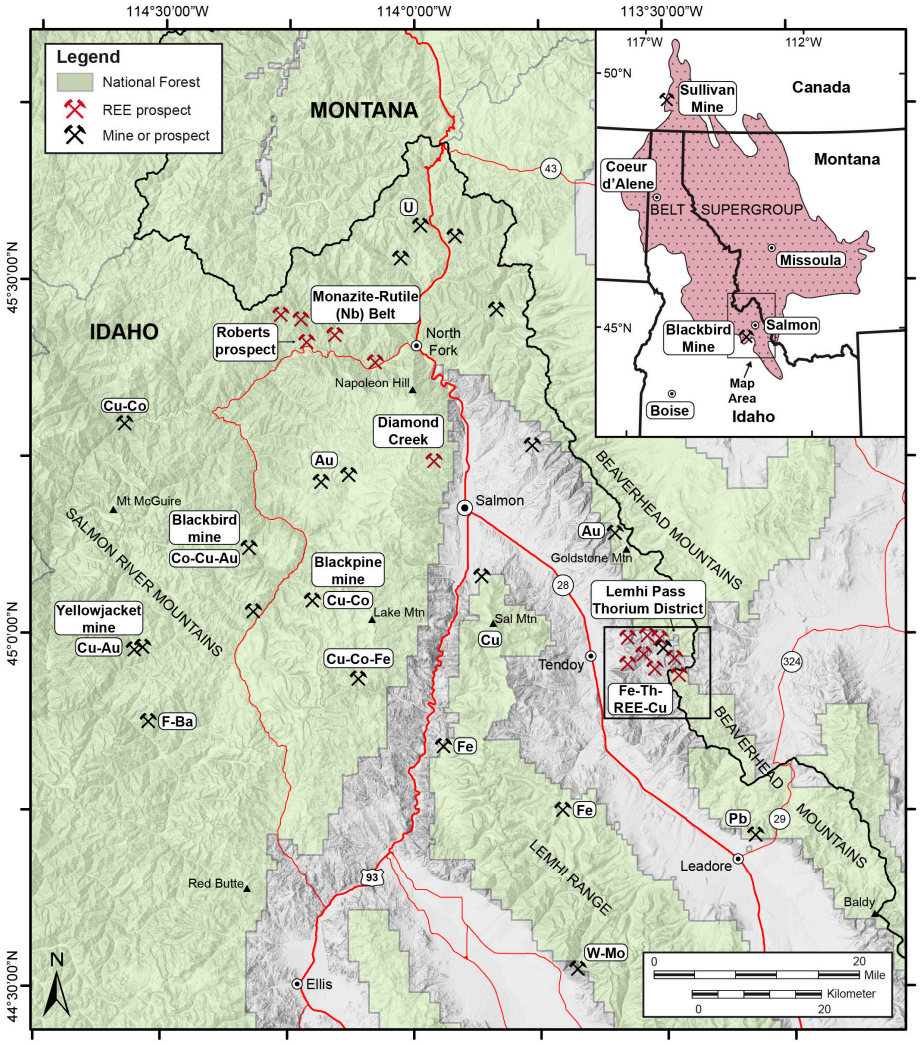


Figure 1. Shaded relief location map for Lemhi Pass District and region. Inset map shows regional extent of 1.4 Ga Belt Supergroup deposition across the states of Idaho and Montana and into Canada. The Monazite–Rutile (Nb) Belt is also known as the Mineral Hill district. Though not shown on the map the belt extends northward into the Sheep Creek drainage of Montana.

Interest in the mineral monazite, a rare earth phosphate with the general formula (Ce,La,Nd,Th)PO_4, has greatly increased in the past two decades. Zi and others [4] provide an excellent description of current understanding of the geochemistry and characteristics of monazite in different geologic environments, including metamorphic and hydrothermal monazites. Their analyses of monazite from multiple settings average about 12 wt. % Nd_2O_3 with some analyses up to about 20 wt. % Nd_2O_3 and a very few at 25 wt. %. At Lemhi Pass, electron probe microanalyses (EPMA) document monazites with 30–35 wt. % Nd_2O_3 consistently. The importance of Nd in modern technology underscores the importance of learning more about these unique deposits and how they formed.

Though small copper veins were exploited in the early 1900s in the Lemhi Pass district, it was not until 1949 that the radioactive thorium-REE lodes were discovered by prospectors looking for uranium. Work by government and industry followed, primarily due to interest in thorium, but the prospecting and research identified significant REEs present as well [1–3,5,6]. Based in part on underground drilling at the Last Chance mine on

the Montana side of the district, Staatz [3] reported an indicated plus inferred resource of about 277,054 metric tons (305,400 short tons) of ThO_2 and indicated plus inferred resource of 279,413 metric tons (308,000 short tons) of total rare earth oxides (REO). The district was declared to be the largest lode resource of domestic thorium in the U.S. and was ranked as such in later studies [7]. Early workers in the 1970s noted a most unusual characteristic of the Lemhi Pass veins, notably that most of the veins sampled had neodymium as the most abundant rare-earth element and europium was also present in anomalously high amounts [2,3].

With few markets at the time for thorium or rare earths, interest in the district waned in the 1980s. The subsequent rise in REE production from carbonatites at the Mountain Pass mine in California and later from Bayan Obo in China satisfied the United States' demand for REEs. In 1972 this Nd-enrichment at Lemhi Pass was only a mineralogical curiosity. By 2010, however, it became more economically interesting as rare earths were increasingly used in a variety of "high-tech" products and devices, including rechargeable batteries for hybrid cars, permanent magnets used in wind turbines, smart phones, defense weapon and surveillance systems, optical fibers, and other essential items which had not even existed three decades earlier [8]. By 2024, REEs were considered "critical minerals" by most governments, due to concentration of supply and high projected future demand. Neodymium was listed on the 2023 U.S. Department of Energy and the 2022 and 2025 U.S. Geological Survey critical minerals list as well as the European Union list of strategic raw materials in 2024, largely due to its use in permanent magnets [9–11]. Industry press releases consider Nd and Pr as prized battery metals which currently fetch higher prices in the market.

Carbonatites are typically enriched in the light rare earth elements (LREE), especially La and Ce, while Pr and Nd are present in lower concentrations, and the heavier lanthanides (or HREEs) are even less common [12]. Ce-monazite is the most common variety of monazite; it is present in carbonatites, placer deposits and as an accessory mineral in granitic and medium-to-high-grade metamorphic rocks. Idaho is one of the few states with historic REE production in the United States; all past production was from placers derived from erosion of the Cretaceous Idaho batholith and related igneous rocks [8,13]. Miners in the 1950s described orange- to yellow-colored monazite in the black sand placers of central Idaho [13].

In contrast, the Lemhi Pass deposits are lodes hosted in Mesoproterozoic siltites, quartzites, and argillites. The weakly metamorphosed clastic sediments were deposited at about 1.4 Ga in the Lemhi subbasin of the Belt basin (Figure 1). Few igneous rocks are present, and Cenozoic volcanics overlie the Precambrian units (Figure 2). Most of the Th-REE-Fe deposits are quartz veins with abundant specular to earthy hematite, thorite, potassium feldspar, and variable amounts of monazite, apatite and other minerals. Supergene oxidation is common. The radioactive outcrops are mixtures of quartz with goethite, wad, and limonite containing thorium oxides as well. A few "replacement" deposits are present in more argillaceous strata which are also highly sheared. These zones are dominated by biotite, specular hematite, apatite, feldspar, thorite, and locally abundant monazite, with minor allanite, muscovite, barite, calcite, and other minerals.

Thorium oxide contents of the larger veins average about 0.4 wt. %, and the Th and REE contents are approximately subequal, though REE contents vary widely among the veins [3]. Staatz and others [2] measured total rare earth oxide (TREO) contents in 31 samples from 21 of the larger Lemhi Pass veins and found the TREO values ranged from 0.073 to 2.24 percent in those 31 samples. They also noted the high Nd contents and unusually high middle rare earth elements (MREE) present in some of the veins over a wide area. In 1979, Staatz [3] concluded that the Th-REE mineralization was related to Cenozoic

faulting and igneous activity, although no deposits are found in Cenozoic volcanic rocks that overlie the Proterozoic strata.

In 2000, when the Idaho Geological Survey first visited the Lemhi Pass district, no geologic or mineral exploration work had been done since 1979. Field work in 2000 and 2006 discovered several unusual and previously undescribed igneous rocks, including a syenite plug and pyroxene lamprophyre dikes. The syenite was dated by U-Pb SHRIMP methods on zircon at 529.1 Ma ± 4.5 Ma [14]. The mafic dikes were initially constrained with Ar^{40}/Ar^{39} geochronology as being older than about 400 Ma. A similar mafic plug was subsequently dated by U-Pb ID-TIMS analysis of zircon at 534 ± 0.22 Ma, or lower Cambrian in age [14,15]. Cross-cutting field relationships show that the igneous rocks predate both copper and Th-REE-Fe mineralization. Regional geologic mapping of the district later helped to better delineate the Proterozoic and Cenozoic stratigraphy [16,17]. Figure 2 is a simplified geologic map of the district. This article focuses only on one aspect of the district—the Nd-rich monazite, its chemistry, and the geochronology with a few observations on possible genesis. While this paper includes much of the previous unpublished work on the Lemhi Pass monazite and REE deposits [14], additional data and interpretations have been added.

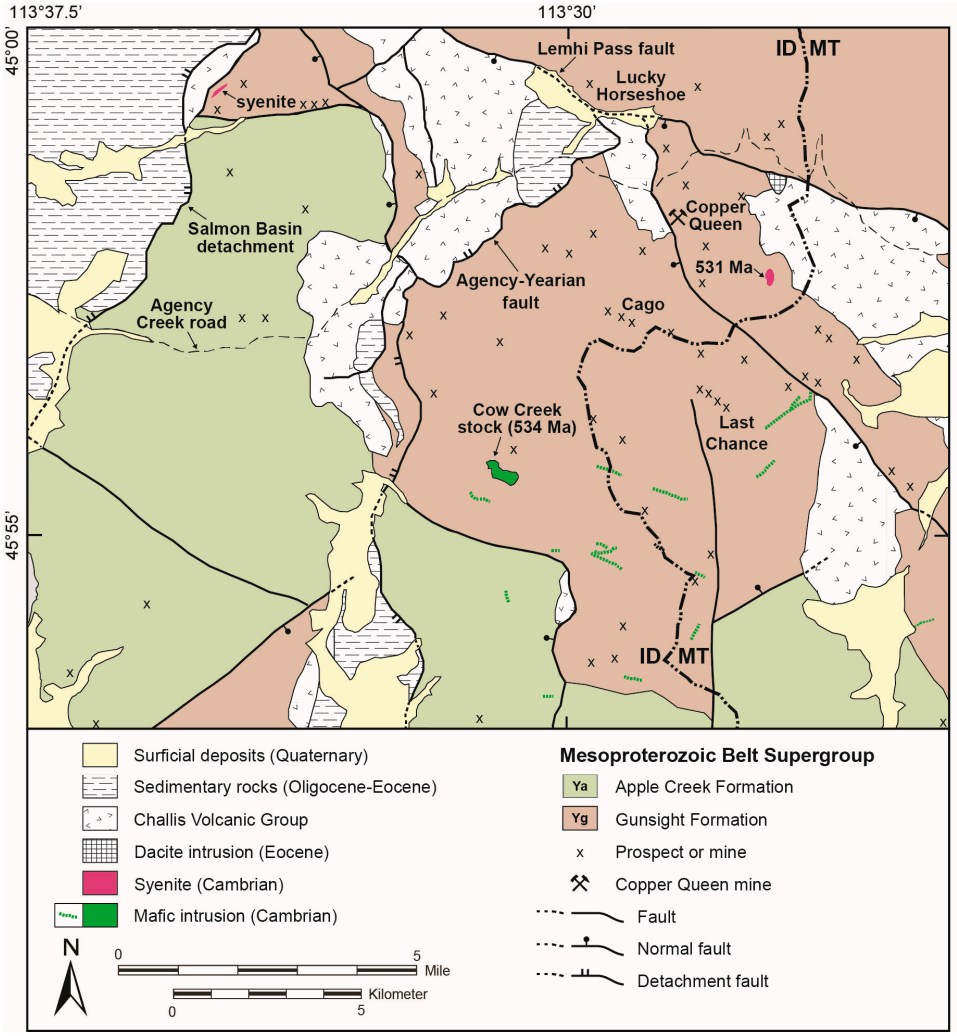


Figure 2. Simplified geologic map of Lemhi Pass district. Modified from Burmester and others [16,17] and Staatz [3]. ID refers to Idaho; MT to Montana, and the state line is labelled.

2. Materials and Methods

2.1. Fieldwork and Chemistry

Standard field mapping and sampling was conducted at many of the larger Th-REE deposits in the Lemhi Pass area in 2000 and again in 2006–2010. Prospect locations and basic descriptions from the literature [3,5] were used to identify the areas of most interest (Figure 2). Detailed trench and pit mapping for selected areas was done to investigate and help sample the mineralogy and wall-rock alteration of the Th-REE veins and deposits [14]. The hazard inventory maps used differential GPS to map mine features in detail, and those maps were used for geology and sample locations as well. The Last Chance mine, the Cago vein, the Buffalo mine, the Lucky Horseshoe mine, the In Trust, the Copper Queen, the Thorium Oxide vein, and the Wonder Lode were the main prospects investigated (Figure 2) [18]. Traverses were made away from mines and prospects to look for regional alteration and structure.

Standard transmitted and reflected light petrography allowed identification of alteration and ore minerals in the deposits. Standard mineral separation techniques (crushing, water table, Franz magnetic separation, hand picking, etc.) were used to concentrate the abundant monazite seen in thin section at the Lucky Horseshoe prospect. However, the separation was difficult until it was recognized that the Lucky Horseshoe monazite grains were light gray in color and did not have the yellow color typical of Idaho's igneous-derived placer monazites. Intergrowths and aggregates of specular hematite and thorite also impeded the mineral separations. Eventually, a combination of Franz magnetic separations, density separations, and manual grain picking allowed selection of suitable monazite grains. The monazite composition was quickly surveyed by SEM methods to confirm mineral identities in grain mounts. Electron microprobe microanalysis (EPMA) was conducted on both grain mounts and in situ on polished thin sections. Monazite in thin section is readily identifiable, and grains were located and marked to facilitate microanalysis. While some large (>200 microns in diameter) grains were present, most monazites were closer to 50 microns in size, making good spatial resolution important for any microanalysis.

Backscattered electron and X-ray compositional maps of a Lucky Horseshoe mineralized section were made in 2025 at the Boise State University (BSU) Isotope Geology Laboratory on a Hitachi TM4000PlusII (Hitachi, Tokyo, Japan) tabletop scanning electron microscope with Oxford Instruments XploreCompact (Oxford Instruments, Oxfordshire, UK) 30 energy dispersive X-ray spectroscopy (EDS) detector and Aztec processing software (Aztec ver. 5.1).

EPMA was used for assessing the detailed chemistry of monazite, with analyses performed both at Washington State University (WSU) and the University of Massachusetts—Amherst (UMass). Mineral compositions for monazite and accompanying silicates and carbonates were analyzed in 2008 at WSU on a Cameca electron microprobe under the direction of WSU Laboratory manager Scott Cornelius, who performed the instrument setup and selected the standards [14]. Additional details of the EPMA analysis at UMass are in Section 2.2 below.

Whole rock chemistry was conducted by two commercial laboratories, ALS Chemex in 2001, and Activation Laboratories in 2008, using standard ICPMS multi-element exploration geochemistry packages for trace elements and REEs. Ore-grade values in two of the 2001 samples were above the limit of the procedure (acid digestion with ICP-MS finish) of 10,000 ppm Nd and 1000 ppm for Pr, Sm, and Th.

Argon geochronology ($^{40}Ar/^{39}Ar$) on biotites and feldspars was conducted at the University of Alaska, Fairbanks, under the supervision of Dr. Paul Layer. Two biotite samples from the Lucky Horseshoe deposit and three potassium feldspar samples from wall-rock alteration zones around the REE-Th veins were analyzed [14].

For the Nd isotopic work, single monazite crystals were spiked with a mixed ^{149}Sm-^{150}Nd tracer, dissolved with 100 µL 6 M HCl in Parr pressure vessels at 180 °C for 48 h, dried, and redissolved in 5 mL 1 M HCl + 0.1 M HF at 120 °C overnight. Bulk rare earth elements were separated by standard dilute HCl and HNO_3 based cation exchange chemistry on 6 mm i.d. × 20 cm columns of AG-50W-X8 resin, H+ form, 200–400 mesh. Sm and Nd were separated by reverse phase HDEHP chromatography on 4 mm i.d. × 10 cm columns of Eichrom Ln-spec resin, 50–100 mesh. Sm and Nd isotopes were measured on an IsotopX Isoprobe-T Thermal Ionization Mass Spectrometer (Isotopx Ltd., Middlewich, UK) in static and dynamic Faraday modes, respectively. Instrumental mass fractionation was corrected with an exponential law relative to ^{146}Nd/^{144}Nd = 0.7219 and ^{152}Sm/^{147}Sm = 1.783.

2.2. U-Th-Total Pb Electron Microprobe Geochronology on Monazite

2.2.1. General Summary

The major REE-bearing mineral phase at Lemhi Pass is monazite. Hence, dating the monazite provides the best evidence for the age of the Th-REE-Fe deposits. In situ studies of monazite textures and chemistry in other studies have documented multiple generations of metamorphic and hydrothermal growth within a single sample [4,19–21]. U-Th-Total Pb dating of monazite with the electron microprobe (EMPA) has the advantage of providing non-destructive compositional mapping and in situ geochronology at a micron-scale, and it has been particularly useful as a means of unraveling complex metamorphic histories when combined with careful petrographic observations and exacting analytical procedures [21,22]. The method is feasible since the monazite lattice typically contains negligible common lead, and the chemical dating must assume that common Pb is minimal compared to radiogenic lead in the dated mineral [22]. Detailed petrographic observation of mineral textures and chemical mapping of the sample is required, and imaged areas of consistent composition (especially for U, Pb, Th) are mapped as specific domains to be dated. Due to the microprobe's excellent (<5-micron spatial resolution), inclusions or thin rims can be distinguished and treated as separate domains for geochronology. While newer in situ methods such as SIMS or LA-ICPMS may offer more discriminating isotopic identification and excellent minimum detection limits, those options were not available when this study was done originally in 2008. EMPA for mapping in this study achieved sub-micron resolution, allowing for chemical mapping and analysis of compositionally consistent domains only a few microns in size, while avoiding any non-monazite inclusions. In this study, the EPMA mapping revealed a small change in Th content of rim and fracture-filling monazite versus the cores and interiors of the monazite grains. As explained below, this corresponded to a significant and geologically reasonable age difference. In addition, the EPMA method offered the potential to identify small, unhydrolyzed domains in thorite, also requiring high spatial resolution for attempts at accurate dating [23,24].

2.2.2. Analytical Procedure for EPMA Geochronology

EPMA monazite mapping and Th-U-total Pb geochronology were performed with the Cameca SX50 and SX-Ultrachron (CAMECA SAS, Gennevilliers, France) instruments at the University of Massachusetts in 2008, using methods specifically developed to enhance Th-U-total Pb geochronology [23]. Analyses were performed on petrographic thin sections as well as grain mounts. For thin section analysis, phases were located by full-thin-section compositional mapping. Once locations were established, the mineral areas were compositionally mapped at higher magnification to reveal internal compositional variation. File S1 lists the general EPMA protocol for monazite in thin sections.

Compositional mapping was done on all monazite and thorite-bearing thin sections and grain mounts using the University of Massachusetts Cameca SX50. This is a 5-WDS

spectrometer instrument (with PGT EDS) with LaB6 cathode, automated via Cameca's SXRayN50 software on a Unix platform. Monazite full section search maps were done using a 15 kV accelerating potential, 200 nA beam current, 35-micron beam diameter, and 35-micron pixel step size. Sections were mapped for Y, Nd (Ce in some cases), Th, and Si. Higher magnification maps of individual monazite grains or areas were done at 15 kV and 200 nA, with pixel dimensions sufficient to generally achieve sub-micron resolution. Elements mapped include Y, Th, U, and Ca. Backscattered electron imaging was done for thorite to determine the least hydrolyzed areas. All quantitative analysis was performed using the UMass CSX-Ultrachron (CAMECA SAS, Gennevilliers, France).

This is also a 5-WDS spectrometer instrument with EDS (Bruker X-Flash SDD), LaB6 cathode and specially modified gun and optics to achieve optimum beam diameter (smallest possible) over a range of voltage and current, with particular attention to the high current, relatively low voltage requirements for EPMA geochronology. This unique instrument also has two specially constructed VLPET (very-large PET) monochromators with commensurately large flow-proportional counters. These spectrometers have approximately 4× the count rates of traditional PET spectrometers. Automation is done via the PC-based PeakSight™ version 3.4 software.

Quantitative analysis of chronometer phases for EPMA geochronology required the measurement of trace concentrations of Pb and U, and for the monazite in the Lemhi Pass area, minor or trace levels of Th. In general, typical metamorphic or igneous monazite contains Th as a major constituent, however the Lemhi Pass monazite is remarkably low in Th overall, and nearly devoid of U, making analysis particularly challenging. In addition, all major elements must be measured in order for accurate matrix corrections to be applied. The PbMα line was used for analysis of Pb. The intensity of PbMα was corrected for overlaps of ThMζ1 and Mζ2, YLγ, and LaLα (2nd order). UMβ was the preferred analytical line for the uranium analysis as the Th interference with UMα is severe. However, Th interference on UMβ still required overlap correction. Background intensities for Pb, Th, and U were obtained by careful WDS scanning (see [23,25]). Scans for each compositional domain were noise filtered, and selected background wavelength regions regressed using exponential modeling (see [21,23] for details). The high concentrations of LREEs in the Pb M region of PET, plus occurrences of other interfering lines, sometimes generated by fluorescence at a distance, required careful evaluation and background modeling to extract appropriate background intensities in monazite.

Thorite is readily rendered metamict due to its very high α-dose, and is then subject to hydrolysis and Pb loss [26]. Thorite analysis proceeded by characterizing each potential grain via backscattered electron imaging to find regions which are not conspicuously hydrolyzed. High backscatter-brightness regions in thorite were found to remain relatively stoichiometric, and Pb loss was expected to be minimized in these areas. Analyses were confined to these regions. For thorite, Th is present in a very high concentration and represents a major element analysis such that radiogenic Pb will reach major element quantities in a few hundred Myr and peak net intensities are expected to be relatively high. Th interference on PbMα is extreme, so the PbMβ line was selected as the analytical line in this case. The other major issue with thorite analysis relates to the uranium analysis. With such highTh concentrations, the absorption edges corresponding to the Th MIV and ThMV levels are significant. The only accurate means of background measurement in this situation is to do a single estimate between the two edges, near the low wavelength side of the ThMγ peak. The Th interference on the UMβ line is substantial but was corrected by interference correction.

The analytical strategy for both monazite and thorite followed that of [27]. Analyses (individual data points) were confined to a defined compositional domain within a grain.

Points were accumulated within the particular domain in order to build an appropriate statistical precision (Figure 3). Histograms were constructed assuming a normal distribution to illustrate age precision. Weighted means of age populations were calculated for an improved estimate of the age when appropriate. A consistency standard (Moacyr monazite, 507 Ma by ID-TIMS and SHRIMP-II) was analyzed before the unknowns were analyzed as a check of calibration and was repeatedly analyzed periodically during each session as a consistency standard [27].

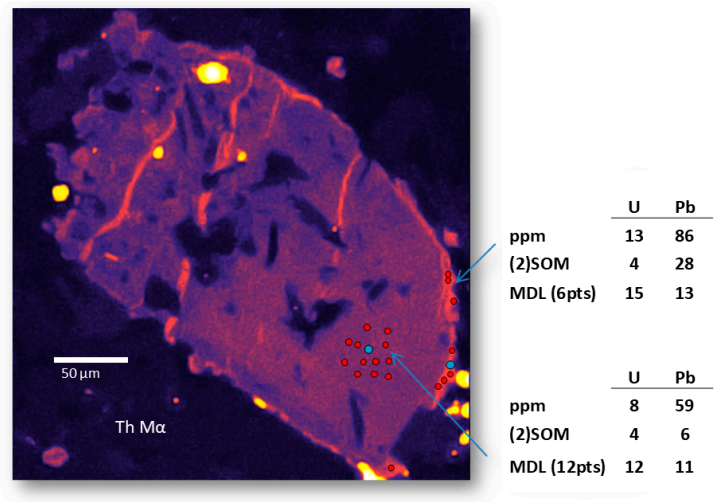


Figure 3. Strategy for quantitative analysis by EPMA showing analytical points superimposed on a Th composition map of a monazite from the Lucky Horseshoe deposit (LH06-25 M3). Brighter colors (red to yellow) indicate higher Th counts. Background point obtained by wavelength scanning is shown in blue and acquired analysis points in red. Achieved concentrations are shown on left with standard error of the mean (SOM), and minimum detectability limits (MDL). Note bright yellow Th-rich areas (thorite) associated with monazite.

Detection limits for the geochronologically relevant elements in monazite and thorite are listed in Table 1 for single-point analyses. Single-point detection limits are compared to population values for monazite in Figure 3. Repeated sampling of a compositional domain was needed in order to improve the statistics for estimation of a single date [27].

Table 1. Single-point detection limits [28] in ppm.

	Th	U	Pb
Monazite	58	30	25
Thorite	755	91	116

3. Descriptions, Compositions, and Age of the REE-Th Deposits

3.1. Field Exposures of the Monazite-Bearing Deposits

3.1.1. Quartz Vein Deposits at the Last Chance and Cago Prospects

For this study, trenches at the Last Chance and Cago veins were mapped and sampled in detail [14]. These are two of the largest Th-REE-Fe mineralized quartz veins; they are approximately 2-m thick and dip steeply to moderately (approximately 45 to 80 degrees), cutting the Precambrian micaceous quartzite host rock (Figure 4). Mineralogy is dominated by quartz, thorite, and specular hematite, largely converted to a mix of red-brown to black secondary oxides. Accessory apatite and monazite are locally accompanied by biotite, barite, carbonate, rutile, allanite, rare fluorite, and other minerals. In outcrop, the quartz displays a peculiar waxy to greasy luster and is strongly stained by iron oxides (Figure 4).

In thin sections, the quartz is cloudy and full of tiny inclusions. The Cago vein and others show a prominent wall rock alteration zone up to a meter wide dominated by untwinned potassium feldspar with minor albite and rutile (Figure 4). The potassium feldspar replaces muscovite in the host quartzite.

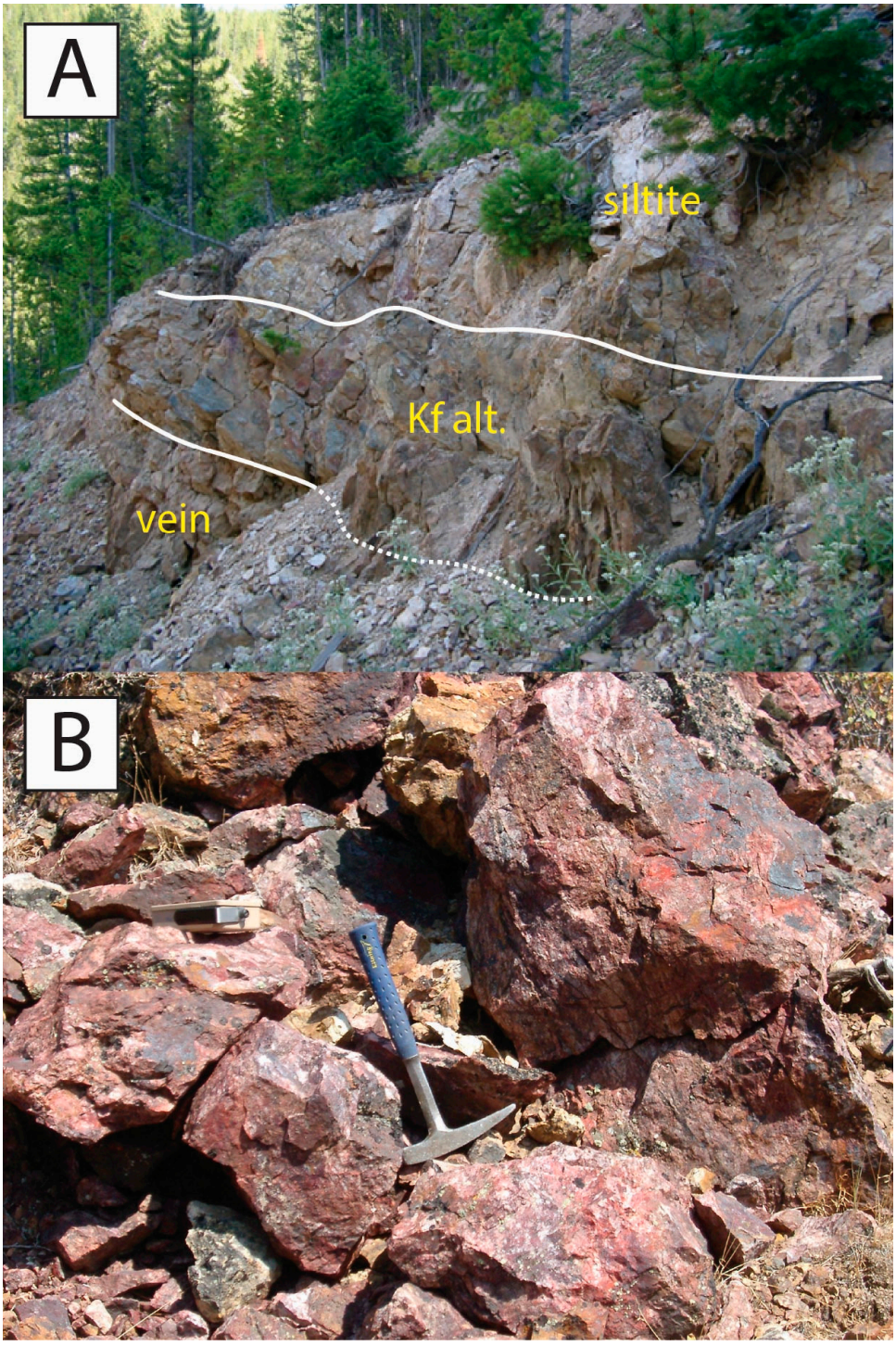


Figure 4. (**A**) Outcrop of Cago vein in trench prior to reclamation. Vein dips to right with potassium feldspar alteration (Kf alt.) in hanging wall. (**B**) Last Chance quartz vein with Th-REE-Fe mineralization from trench. Colorful red to brown oxides are typical.

3.1.2. Lucky Horseshoe Shear Zone Deposit

The Lucky Horseshoe deposit is exposed in a small open pit, and the mineralized zone was apparently protected from supergene oxidation by thick colluvium and soil.

The Lucky Horseshoe mineralized zone is unusual compared to most other prospects in the district, forming a cataclasite breccia to local mylonite and replacement zone along what is interpreted as a flat-lying shear zone (Figure 5). Though previously mapped as a vein by Staatz, the deposit has been partially excavated and disrupted, thus any vein noted by Staatz is not visible [14,18]. The lack of a vein, mylonite, or radioactivity in an adit driven under the surface exposure is further evidence that the deposit consists of a flat-lying, biotite-rich shear zone which may be folded and continue southward to nearby prospects [18]. Dominant minerals are hematite, potassium feldspar, brown biotite, monazite, and thorite. Green biotite, muscovite, albite, apatite, allanite, barite, fluorite, and minimal quartz and carbonate are present locally. Samples from the Lucky Horseshoe had some of the highest REE contents (0 to over 10 wt. % by XRF spectroscopy) noted in early studies [2,3,29]. The Lucky Horseshoe is unique in not being affected by supergene secondary oxidation, and that plus its abundant monazite made it a focus of this research.

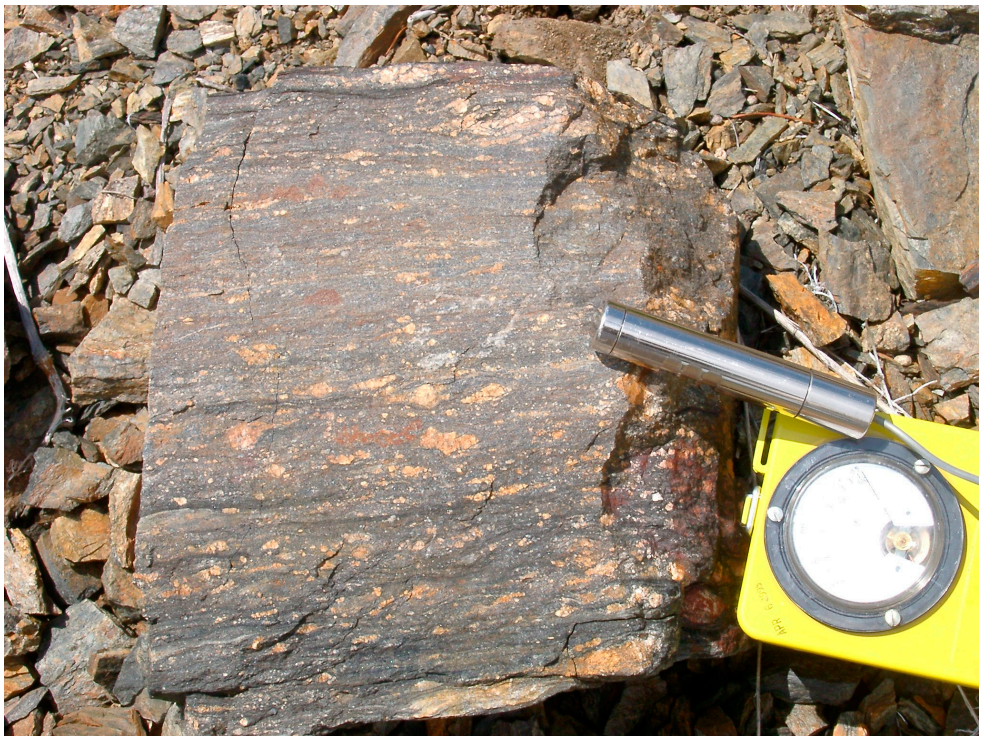


Figure 5. Sample of Lucky Horseshoe cataclasite with Th-REE-Fe mineralization. The tan porphyroblasts are feldspar. The sense of shear, though possibly dextral on this piece, is not consistent in outcrop, though more detailed work is needed. Both compressive and extensional events have been mapped in the region.

In thin sections, a schistose-to-mylonitic fabric is evident in the orientation of the biotite grains. Some biotite layers contain an estimated 20% monazite, as well as opaques, specular hematite, and thorite (Figures 6 and 7). In places, the monazite grains, which are 10–100 microns long, appear to form porphyroblasts growing across the foliation, though the timing of mylonitization and mineralization is difficult to ascertain. The preferred interpretation is that both were synchronous in part. Clasts of flattened and broken feldspar are common, and one possible interpretation is that they are remnants of syenite which was intruded along the shear zone. A minor late retrograde event is suggested by sparse veins and replacements of chlorite and sericite.



Figure 6. Transmitted light photograph of standard-size thin section KCV-5 from Lucky Horseshoe deposit (LH-8a). Tiny white grains in the upper, brown portion are monazite in the biotite-rich layer (brown). Length of section is approximately 4.5 cm.

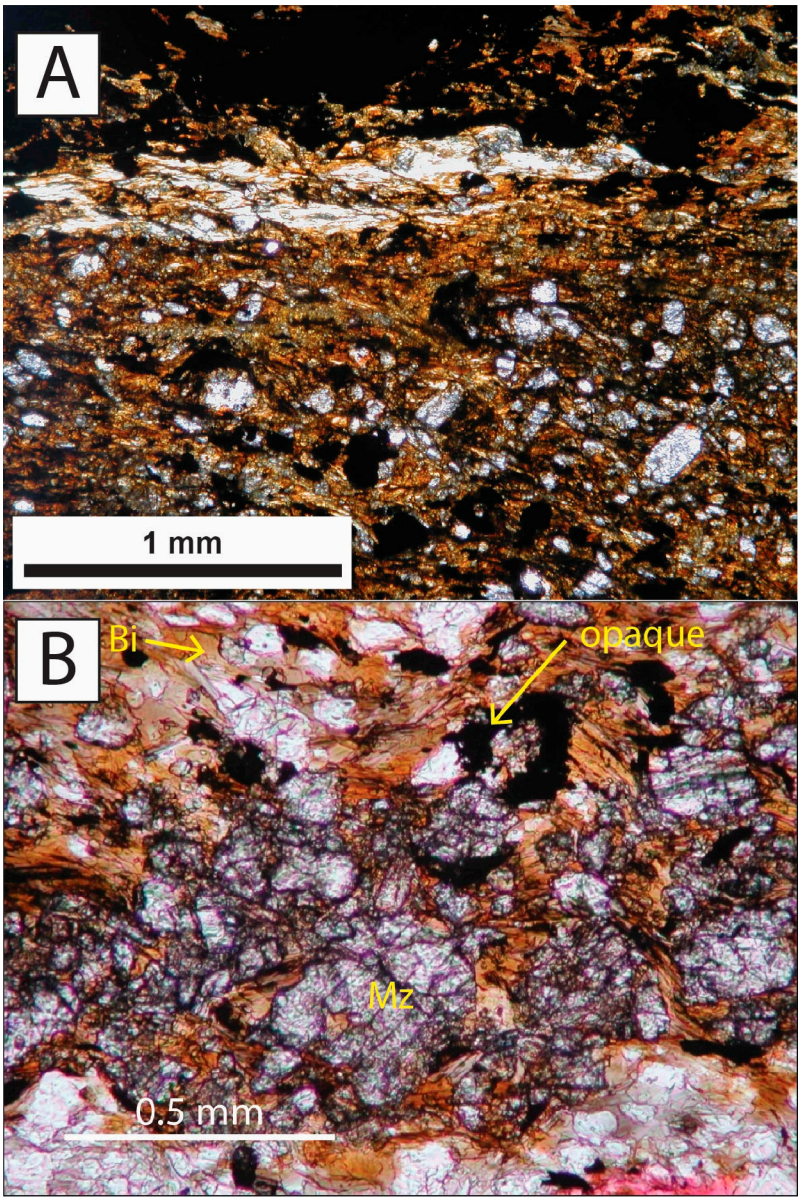


Figure 7. (**A**) Lucky Horseshoe mineralization in plane-polarized transmitted light with colorless monazite grains abundant in brown biotite-rich layer in lower half of image. Sample LH-12, section kcv-9. (**B**) Enlarged view of monazite (Mz) and biotite (Bi) intergrown with opaques (specular hematite and thorite), section LH-12c2.

Textures of the Lucky Horseshoe rocks show that the hematite, monazite, and thorite phases coexist and appear to belong to the same stage of mineralization (Figure 8).

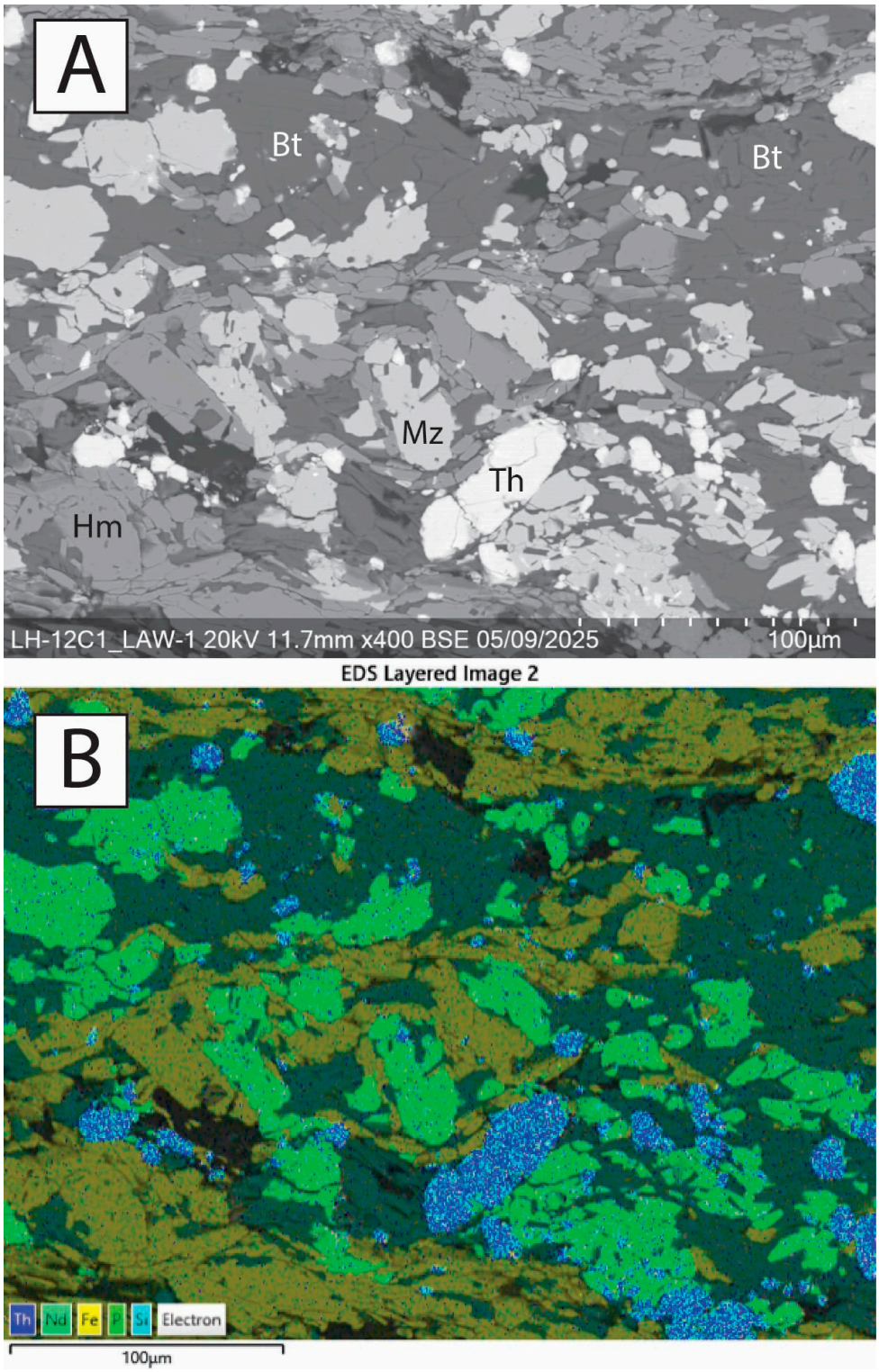


Figure 8. (**A**) SEM-BSE image of LH-12C1 (LAW-1 section) with minerals labelled as monazite (Mz), thorite (Th), biotite (Bt), and hematite (Hm). (**B**) Compositional map as layered SEM EDS image for same Lucky Horseshoe sample. Elements distinguish the four minerals shown by colors in legend at lower left corner.

3.1.3. Field and Argon Geochronology Constraints on Timing of REE Mineralization

Field work and prior literature studies constrained the REE-Th-Fe veins and lode deposits to younger than the ~1.4 Ga Mesoproterozoic host rocks and older than unmineralized Eocene volcanic and conglomeratic units which overlie the district. Staatz [3] and other workers noted a sequence of three vein types in the district: early quartz–chalcopyrite veins, barren hematite veins, and the REE-Th-Fe veins, all hosted primarily by the Mesoproterozoic metasedimentary rocks. In the Copper Queen mine, Schipper [30] described copper mineralization within mafic rocks, and workers also mapped a cross-cutting "radioactive veinlet that is later than the copper" [6,30]. The quartz-copper veins are cross-cut by low-angle faults interpreted to be related to Cretaceous thrusting in the region [14]. Several of the Th deposits contain minor copper, consistent with the hydrothermal fluids which precipitated REEs having interacted with and remobilized some of the earlier copper. A specular hematite vein cuts a nearby syenite plug (Figure 2), and hematite is locally interstitial to the feldspar crystals in the syenite, suggesting that the REEs also post-date intrusion of the syenite [14].

Dating of the syenite by U-Pb SHRIMP analysis of zircons at 529.1 Ma ± 4.5 Ma [14] and of the pyroxene porphyry south of the district by U-Pb ID-TIMS analysis of zircons at 534 ± 0.22 Ma [15] clearly identified the magmatic rocks as early Cambrian.

Three samples of potassium feldspar from three different REE-Th veins (the ThO_2 vein on the outer part of the district; the Lucky Horseshoe, and the Cago vein) were dated by $^{40}Ar/^{39}Ar$ methods at the University of Alaska, Fairbanks. Each sample had a complex, disturbed spectra with a (reset) saddle age of approximately 56–112 Ma, stepping up to a maximum age of 175 to 230 Ma [14]. Closure temperatures of the Ar system in potassium feldspar are approximately 150 °C to 350 °C, and the ages represent the age of cooling below the closure temperature.

Samples of igneous-related hornblende returned a disturbed age of greater than 400 Ma for Copper Queen mafic lamprophyre and a plateau age of 558 Ma for a pegmatitic breccia south of the main district [14]. An earlier attempt to date biotite at the Lucky Horseshoe was unsuccessful as the sample was partially reset. None of the other REE deposits have significant biotite.

In summary, field relations, along with U-Pb ages of igneous rocks and $^{40}Ar/^{39}Ar$ geochronology clearly constrain the main REE-Th-Fe lodes to younger than Cambrian and older than about 200 Ma. Partial resetting of the feldspars likely took place between 50 and 110 Ma, based on the saddle age observed in the argon spectra.

3.2. Lemhi Pass Rock Geochemistry

The unusual pattern of the rare earth chemistry of the Lemhi Pass deposits is evident in whole-rock analyses from earlier workers as compared to those compiled in literature summaries [31]. Early workers recognized the high Nd content and the more abundant middle rare earths (MREE, used here to mean Pr through Gd) as compared to the typical LREE-enrichment (especially La and Ce) in carbonatites and Ce-monazites in placer deposits [2,12]. Staatz et al. [2] analyzed 31 samples from 21 veins in the district using a combination of wet chemistry and X-ray fluoresence methods. They reported total rare earth oxide (TREO) values ranging from 0.073 to 2.24 weight percent with an average TREO of 0.43 wt. %. TREO to ThO_2 ratios varied widely from 0.05 to 9.2. The average ThO_2 content was 0.51 wt. % for the 31 samples. The samples were primarily chip samples with a few channel samples and grab samples included and likely taken to be representative for the government assessment. Their highest-grade sample was from the Lucky Horseshoe deposit, and it assayed 2.24 wt. % TREO, including 1.37 wt. % Nd_2O_3 plus 0.149 wt. %

Pr_2O_3 and 0.157 wt. % Sm_2O_3. Their results include multiple 0.05 to 0.1 wt. % Nd_2O_3 analyses for the whole-rock vein samples.

Gibson [29] and Gibson and Wood [32] also looked in detail at the mineralogy and chemistry of the deposits and documented their unusual high middle rare earth (MREE) enrichment. Trenching in 2023 as part of mineral exploration activities at two other prospects (In-Trust and Sparky) recovered samples with similarly high Nd concentrations [33]. The strong REE mineralization (9000 to over 30,000 ppm TREE) included some samples in which Nd accounted for over 50% of the REE suite [33]. Mineralization was generally associated with faults, but much of the areas trenched are mantled with colluvium, and the detailed geology is not obvious from surface exposures.

Comparisons to estimated crustal abundance and other domestic and global REE deposits demonstrate how uncommon Lemhi Pass' high Nd proportion is for REE deposits [31]. A chondrite-normalized REE spider plot of six Lemhi Pass samples from three different deposits demonstrates this unusual geochemical distribution at Lemhi Pass (Figure 9). Four of the six samples show Pr and Nd values more enriched relative to chondritic values than La or Ce, which are the most abundant rare earths globally and in most carbonatites. The other two Lemhi Pass samples have peaks at Sm and Eu.

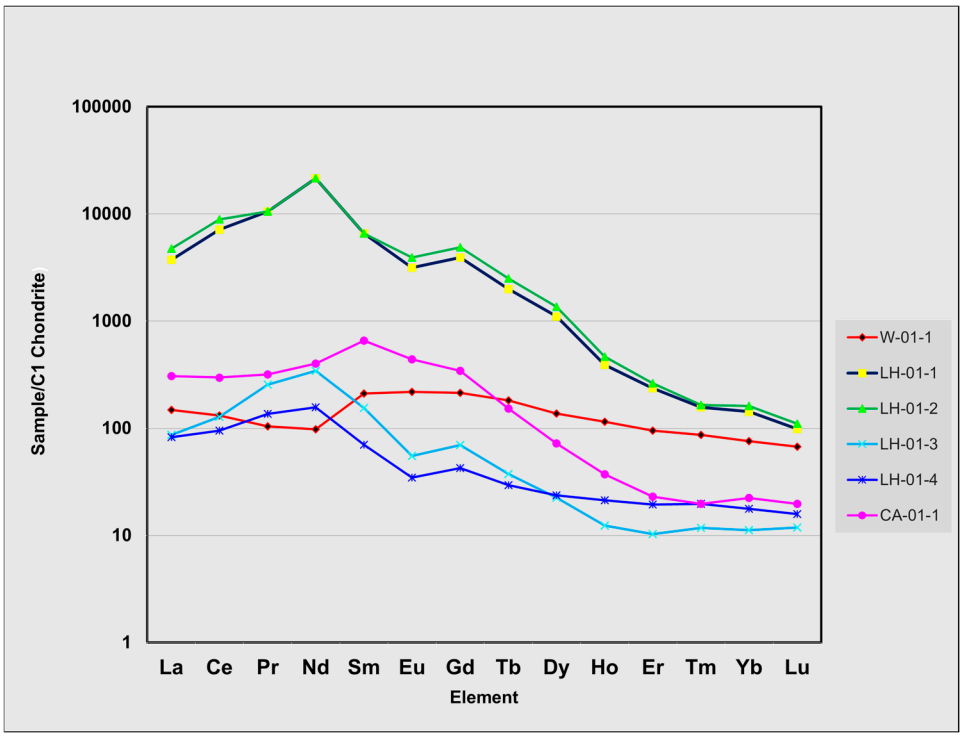


Figure 9. Chondrite-normalized plot of whole-rock rare earth contents for six samples from Lemhi Pass district. LH is Lucky Horseshoe, W is Wonder lode, CA is Cago vein. Nd values plotted were capped at the upper analytical limit of 10,000 ppm for LH-01-1 and LH-01-2. Pr, Sm, and Th values were capped at 1000 ppm, the upper analytical limit.

Table 2 shows the REE contents of whole-rock analyses of two high-grade REE samples [14]. A sample from the Lucky Horseshoe deposit (LH06-24B) at Lemhi Pass is compared with a high-grade carbonatite sample (07WP127B) from the Mineral Hill district and the syenite from Lemhi Pass [14]. The syenite is modest in its REE contents and shows Ce and La to be more abundant than Nd.

Table 2. Whole-rock REE analyses for selected Lemhi County rocks [14]. All data reported in ppm.

Element	Lucky Horseshoe, Lemhi Pass (LH06-24B)	Roberts Carbonatite, Mineral Hill (07WP127B)	Syenite, Lemhi Pass (JA06-01)
La	658	87,500	180
Ce	4920	113,000	325
Pr	1430	9950	39
Nd	8350	23,300	119
Sm	1220	1300	20
Eu	165	210	3
Gd	448	208	16
Tb	24	16	3
Dy	60	66	14
Ho	9	11	3
Er	29	34	9
Tm	0	4	1
Yb	7	14	9
Lu	0	0	1
Th	2510	2810	33
U	18	11	7
TREE	17,320	235,614	741
Ce/Nd	0.59	4.85	2.73

The high-grade carbonatite sample (07WP127B) is typical of mineralized carbonatites with percent levels of REEs and La and Ce in much greater abundance than Pr, Nd, or the heavier REEs. The carbonatite sample has higher total REEs, which may be hosted in multiple minerals, including monazite but also bastnasite or related carbonate minerals. The sample from Lemhi Pass has a lower total REE content but La is very low (depleted?), and the Ce/Nd ratio is below 1. Nd has by far the highest concentration of the individual REEs This particular Mineral Hill carbonatite sample displays coarse, honey-colored Ce-monazite plus calcite, apatite, and actinolite, while the Lucky Horseshoe REEs are contained in the less abundant, very fine-grained, Nd-enriched monazite (Figures 6–8). The syenite sample is only modestly enriched in REEs overall and it contains more La and Ce than Nd, as is typical of igneous rocks.

3.3. Monazite Chemistry

Standard SEM-EDS analysis allows efficient identification and determination of semi-quantitative monazite compositions. Figure 10 shows an EDS spectrum for a Lucky Horseshoe monazite (LH06-24B) and for comparison, a Ce-monazite from a REE-bearing carbonatite (07WP127A) in the Mineral Hill district, located about 70 km to the northwest of Lemhi Pass. The Mineral Hill carbonatites show the typical monazite pattern with Ce peaks dominant over La [34]. In contrast, the Lucky Horseshoe and other Lemhi Pass monazites are quite distinct with a very strong Nd peak that is approximately twice as high as the Ce peak and a very low La peak. While not fully quantitative, the pronounced high and sharp Nd peak on SEM-EDS analysis, indicates the extreme Nd-enrichment in these monazites.

Monazites in polished thin sections from the Lucky Horseshoe deposit at Lemhi Pass were analyzed by electron microprobe along with a monazite from the Roberts carbonatite deposit in the Mineral Hill district and monazite in a section from the Sunshine Lode of the Blackbird Copper-Cobalt District (Figure 1). Results, tabulated as oxides, are in Table 3. The eight Lucky Horseshoe monazites were very consistent in composition with Nd oxide contents ranging from 34.77 to 36.59 weight percent and averaging 35.5 wt. % Nd oxide. Ce oxide is approximately 15 to 16 wt. % for the Lucky Horseshoe samples, but about 32 wt. % for the two other samples. The Lucky Horseshoe monazites also contain

La oxide at 2.5–3.5 wt. %, Ce oxide about 16 wt. %, Pr oxide about 5.5 wt. %, Sm oxide 3 to 5 wt. %, and 1 wt. % or less of Y, concentrated in specific domains. Eu oxide is about 1.3 wt. %. File S2a,b contains the full analyses along with cation assignments and statistics. Compositional mapping revealed the presence of low and higher Th domains in the Lucky Horseshoe monazites (Files S3 and S4), but the compositional variation in Nd_2O_3 and the other rare earth oxides is quite low.

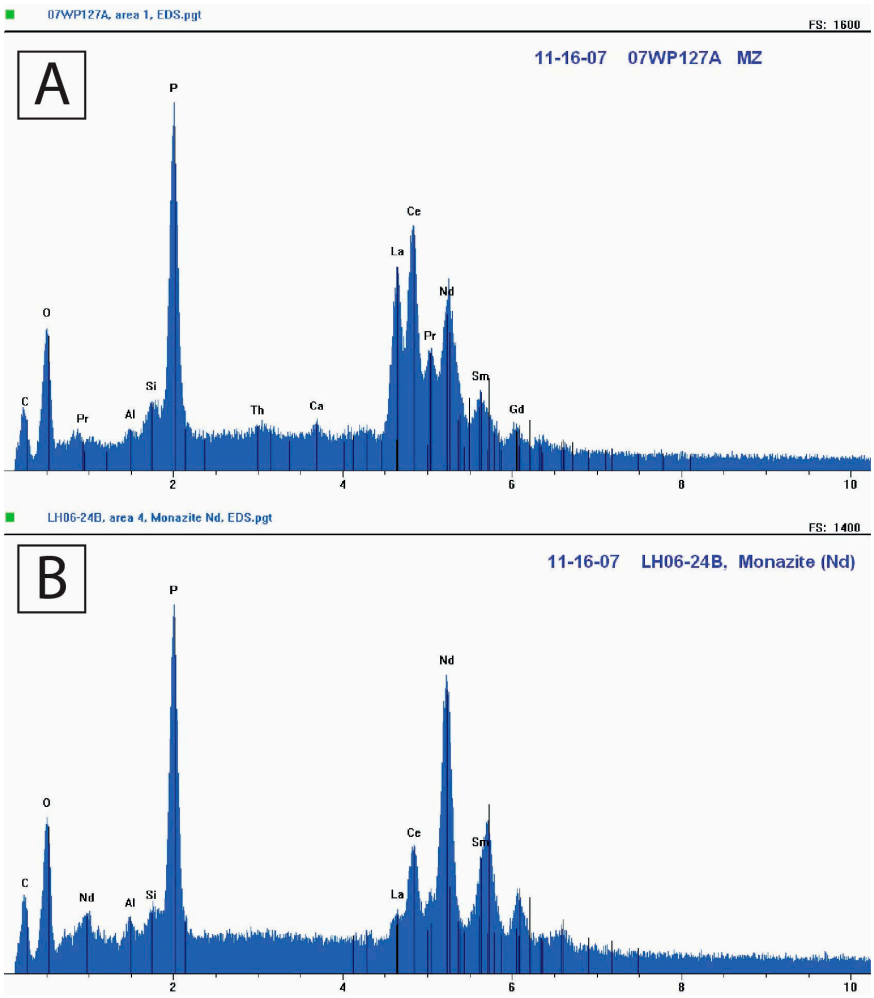


Figure 10. SEM EDS spectra for monazites at (**A**) the Roberts carbonatite prospect in the Mineral Hill district (07WP127A), and (**B**) the Lucky Horseshoe deposit (LH06-24B).

Table 3. Monazite compositions by EPMA, analyzed at WSU or by compositional domains of Th, Y at UMass on the SX-Ultrachron. The Sunshine Lode sample is from the Idaho Cobalt belt and the Roberts S sample is a carbonatite. LH is for Lucky Horseshoe deposit at Lemhi Pass. Concentrations shown are averages of multiple spot analyses per sample.

Monazite Sample (Wt. %)	LH12c2	LH06-24A	LH-8a	LH-12	LH12c M2 Low Th	LH12cM2 High Th	LH06-25 M3 High Y Core	LH06-25 M3 High Th Fracture	Sunshine Lode	Roberts S (07WP127B)
Y_2O_3	0.88	0.62	0.44	0.81	1.15	0.80	1.38	0.61	1.09	0.03
La_2O_3	3.40	2.77	3.44	3.63	3.68	3.49	2.42	2.95	13.89	25.18
Ce_2O_3	16.19	15.16	16.25	16.67	16.87	16.42	14.28	15.77	31.39	32.87
Pr_2O_3	5.44	5.50	5.50	5.58	5.03	5.02	4.94	5.13	4.23	4.10
Nd_2O_3	34.94	36.59	36.38	35.17	34.77	35.10	35.78	35.46	12.86	6.71
Sm_2O_3	5.01	5.08	4.77	4.89	2.94	2.93	4.24	3.76	2.40	0.30
Eu_2O_3	NA	NA	NA	NA	1.21	1.18	1.47	1.34	NA	NA

Table 3. *Cont.*

Monazite Sample (Wt. %)	LH12c2	LH06-24A	LH-8a	LH-12	LH12c M2 Low Th	LH12cM2 High Th	LH06-25 M3 High Y Core	LH06-25 M3 High Th Fracture	Sunshine Lode	Roberts S (07WP127B)
Gd_2O_3	1.43	1.32	1.40	1.52	1.56	1.61	2.08	1.84	2.14	0.58
ThO_2	0.63	0.56	0.49	0.52	0.48	1.84	0.50	1.81	0.26	0.65
UO_2	0.09	0.09	0.09	0.09	0.00	0.00	0.00	0.00	0.22	0.11
PbO	0.08	0.17	0.15	0.18	0.01	0.01	0.01	0.01	0.17	0.09
CaO	0.31	0.15	0.31	0.16	0.23	0.35	0.31	0.23	0.08	0.09
SiO_2	0.32	0.35	0.22	0.16	0.20	0.24	0.23	0.29	0.34	0.00
Al_2O_3	0.05	0.08	0.01	0.01	NA	NA	NA	NA	0.24	0.00
P_2O_5	29.29	29.13	29.49	29.49	28.87	28.96	29.60	29.83	29.87	30.49
Oxide Totals	98.05	97.57	98.94	98.90	97.98	98.81	98.08	99.87	99.19	101.17
TREO (La-Gd)	66.40	66.41	67.73	67.48	66.07	65.74	65.20	66.26	66.91	69.73

3.4. Monazite and Thorite Geochronology

Samples of monazite mineral separates and polished sections from the Lucky Horseshoe deposit were analyzed for U-Th-total Pb EPMA geochronology [14]. Thorite, which coexists with monazite in the deposits was also analyzed, as imaging revealed zones which were not metamict or hydrolyzed [14]. In general, both minerals returned a bimodal age distribution with broad zones in the mid-Paleozoic and a discrete set of ages in the Cretaceous as well. No evidence of either Precambrian or Tertiary ages were found. Results from a single monazite grain and then a single sample (LH-06-025) are presented first to illustrate the methodology and the details for the multiple spot analyses from a single sample. A probability histogram of the full dataset of both monazite and thorite is presented subsequently. Summary results for monazite are tabulated in File S5 and for thorite in File S6.

The X-ray compositional maps of monazite grains showed volumetrically tiny rims and fracture fillings of higher Th content, and cores of low to high Y content (Figure 11, Files S3 and S4).

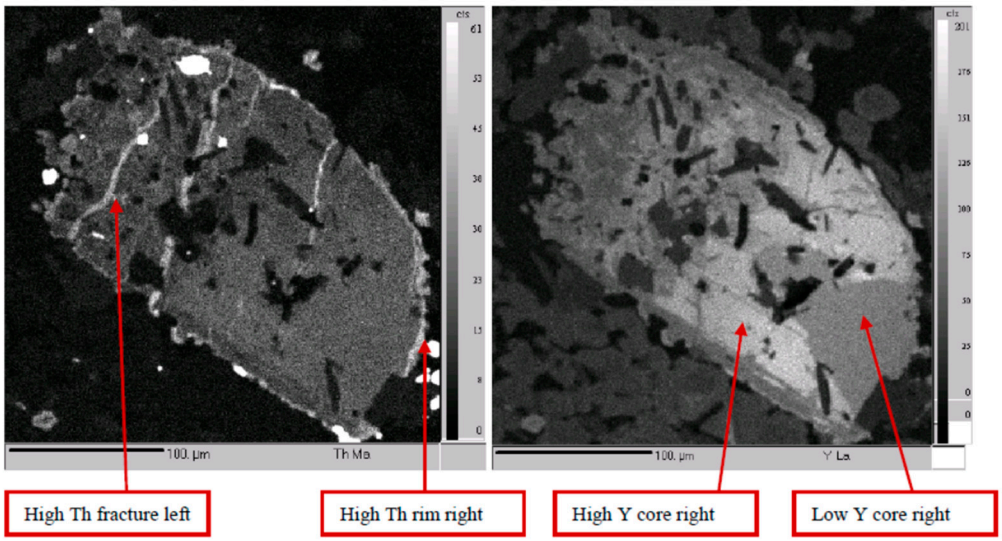


Figure 11. X-ray compositional maps of monazite grain M3 from sample LH06-25, Lucky Horseshoe deposit. Th map is on left; Y map is on right. The small, very bright white areas in the Th map are inclusions of thorite. Compositional domains are identified by higher and lower Y contents on right image, and by higher and lower Th contents on left image. Analyses in Table 3 show minimal differences in the Nd values between the zones. The original image which displays similar maps of many grains is in File S3.

Monazite geochronology results for the monazite grain M3 shown in Figure 11 are in Figure 12. The graph combines the spot analyses for all domains within grain M3 with domains of grain M2; both grains are from the single sample (LH06-25). Figure 12 distinguishes results for the compositional domains (based on Th and Y contents) as well as the delineation of core and rim zones visible in Figure 11 and Files S3 and S4. The histogram in Figure 12 and the numerical data sets reveal a clear bimodal to possibly trimodal array of ages that span a broad range from about 430 Ma to about 80 Ma. However, there are two major groupings for the monazite ages, one with peaks at approximately 350 Ma and a secondary peak at about 280 Ma, versus one much younger, discrete grouping near 100 Ma. The Cretaceous ages are confined to the thin rim and fracture-fill zones visible in the X-ray compositional monazite maps in Figure 11. The younger rim monazite contains higher Th contents (Table 3).

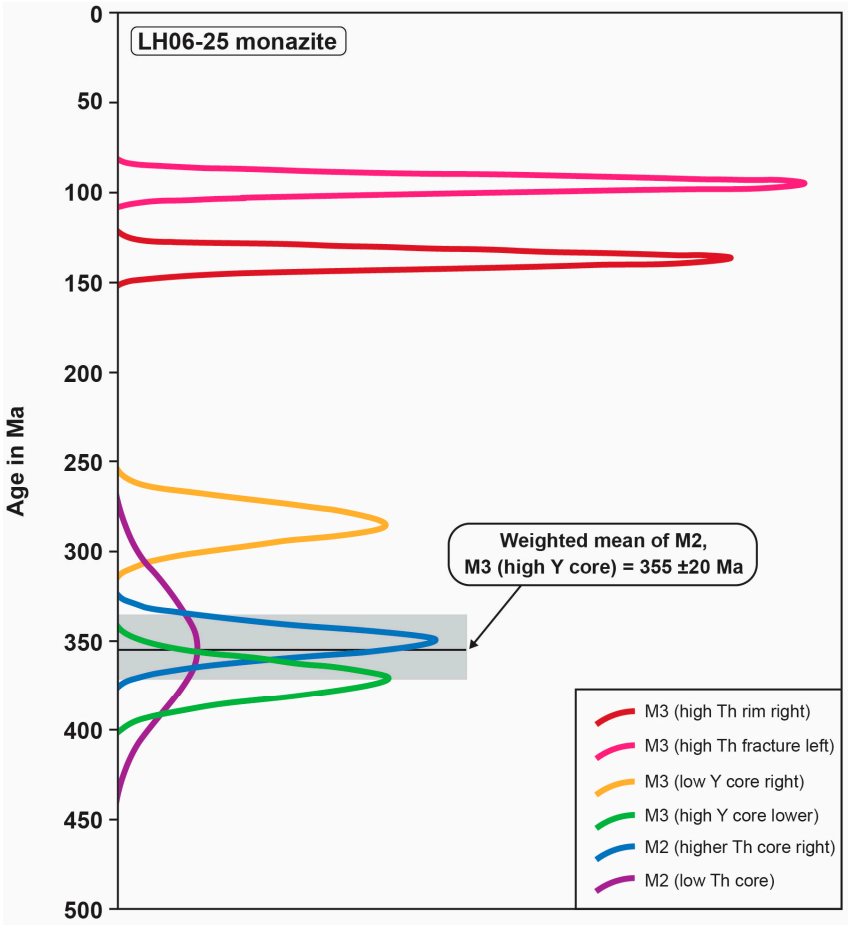


Figure 12. Histogram of age results on monazite from single sample LH06-25, Lucky Horseshoe deposit, Lemhi Pass. Curves are Gaussian representatives of probability distribution for a single-date (6–12 points each) showing 2-sigma weighted error. Note that the weighted mean calculation shown does not include the low Y core (yellow line) due to its textural and compositional distinction.

The ages determined for LH06-25 are scattered but clearly define two broad intervals of Phanerozoic time. The older grains returned ages from about 450 to 250 Ma with the most precise values close to 350 Ma. A weighted mean of the cores from two grains (M2 and M3 high Y core) is 355 Ma ± 20 Ma, placing their crystallization in Late Devonian to Early Mississippian time. Cores, evident in Figure 11, display some zoning in their Y content. In this sample the lower Y core is somewhat younger in age (ca. 280 Ma) than the higher Y core (ca. 364 Ma). The circa 280 Ma age could represent another hydrothermal event, as it is also present in the thorite data. Importantly, the monazite cores are much

older than the high Th rims and fractures of monazite deposited between approximately 150–80 Ma during the Cretaceous. While the histogram and data fit nicely into the two distinct broad age ranges (Paleozoic and Cretaceous), it is unclear how much of the time range is due to analytical or random mineral composition variations versus real ages of crystallization during a lengthy span of hydrothermal activity. The EPMA method assumes that monazite does not contain common lead. If there was a component of common lead in addition to the radiogenic lead, the true age (assuming no lead loss) would be younger than the measured age. Hence, it is difficult to shift the mid-Paleozoic age determinations back 150 my to match the early Cambrian pluton ages.

Geochronology on thorite is more challenging as thorite is easily affected by supergene weathering and often metamict due to the high thorium content. The thorite results as well as the full suite of monazite results are shown in Figure 13. At Lemhi Pass, the EPMA geochronology of both monazite and thorite return broadly consistent bimodal populations of Paleozoic and Cretaceous ages (Figure 13; Files S5 and S6). Results from five thorite samples are more scattered but agree with the two main time intervals of 400 to 280 Ma and 200–100 Ma for crystallization (Figure 13), lending support to the monazite determinations of Paleozoic Th-REE-Fe mineralization. Thorite grains analyzed for this study were selected to avoid metamict or hydrated grains or zones, and overall, the ages are quite similar to the monazite ages [14,24]. It is unknown if the greater dispersion is due to alteration and metamictization in the thorite, or possibly reflects continued hydrothermal activity at lower temperatures.

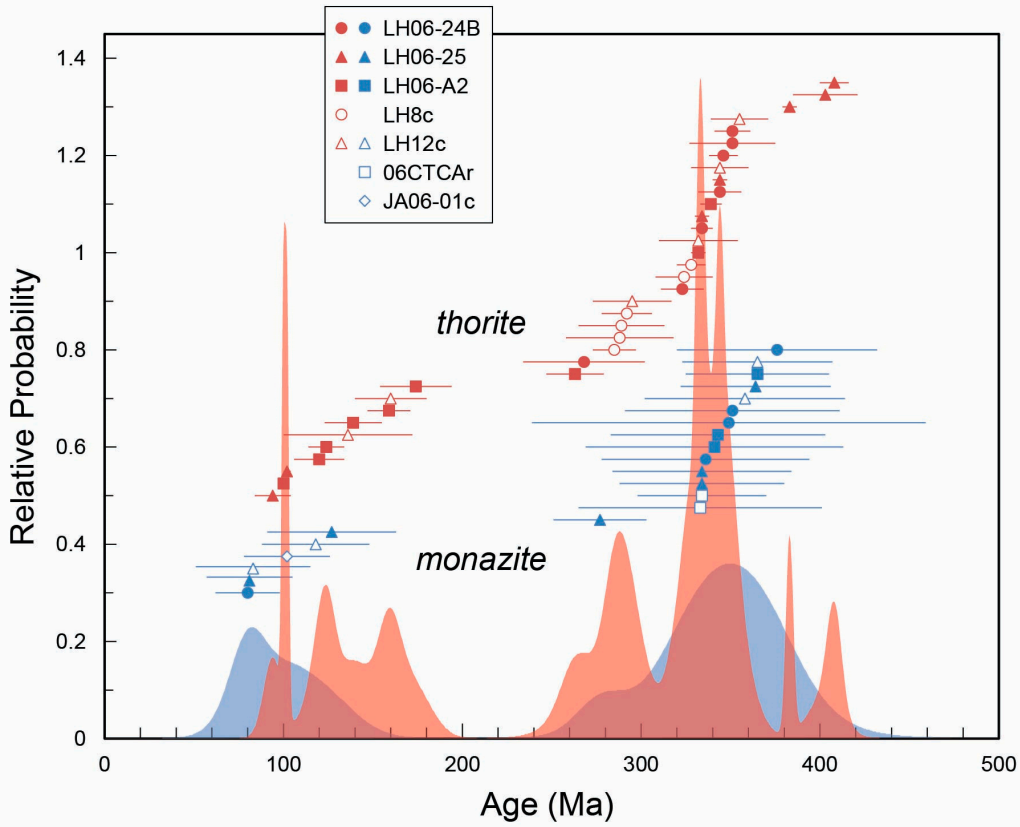


Figure 13. Ranked EPMA Th-U-total Pb dates with relative probability density functions for monazite and thorite domain analyses from all Lemhi Pass samples analyzed in this study [14]. Ranked dates illustrated with 2 SOM error bars. Geochronologic data is in File S5 (monazite) and File S6 (thorite). Monazite analyses and probability density function are in blue. Thorite analyses and probability are in red.

3.5. Isotopic and Chemical Evidence

Three single crystals of monazite mapped as relatively homogeneous in composition by WDS X-ray techniques were analyzed by ID-TIMS for Nd isotopes (Table 4). Present-day Epsilon Nd values are −6.2 to −6.8, and initial values at a crystallization age of 355 Ma are −1.8 to −2.2 (Figure 14). Two-stage depleted mantle model ages were calculated using the Sm/Nd of the North American Shale Composite of [35] for the evolution of a sedimentary rock source prior to mineralization, resulting in model ages of ~1.35 Ga. These isotope ratios require a mixture of mantle-derived and incompatible-element-enriched crustal sources for the rare earth elements making up the Lemhi Pass monazites. The most obvious potential crustal sources are the Mesoproterozoic Belt Basin metasedimentary rocks and the suite of 1370 Ma augen gneisses and megacrystic granites which intrude them (Figures 1 and 2; [36]). A study of common lead isotopes in ore and alteration minerals at Lemhi Pass and elsewhere in the region also indicated significant interaction with radiogenic crustal rocks such as the Mesoproterozoic Belt Supergroup sediments or other ancient basement gneisses [14,37,38].

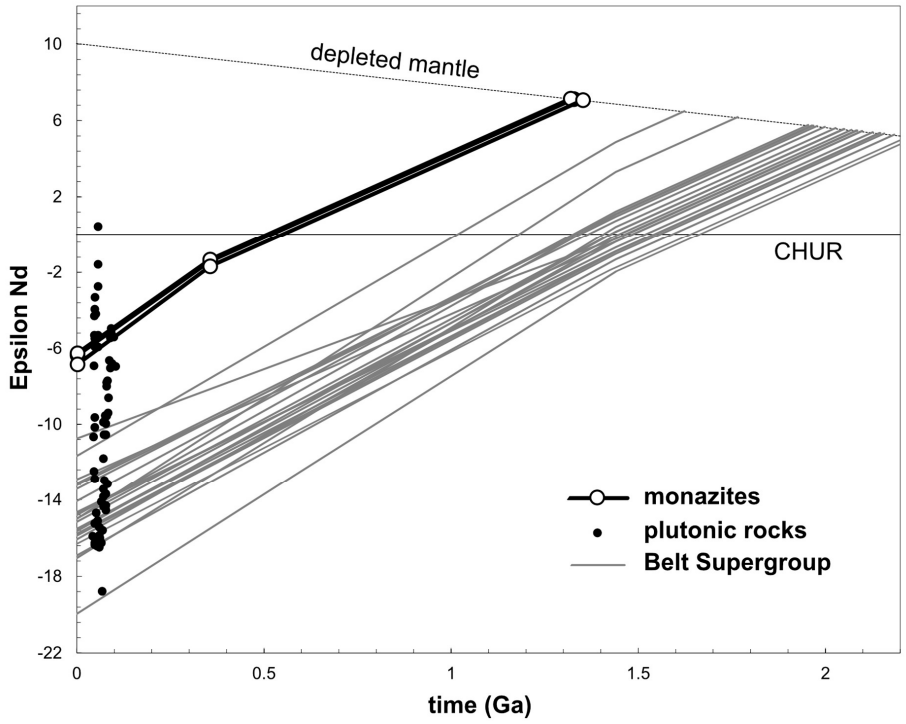


Figure 14. Nd isotope evolution diagram showing two stage depleted mantle model ages for three single monazite crystals, with respect to the evolution of Belt Supergroup fine- and coarse-grained sedimentary rocks [39] and Phanerozoic intrusive rocks of the Idaho Batholith and Challis Intrusive Province [40].

3.6. Temperature Estimates and Fluid Composition

Three fluid inclusion or mineral geothermometry studies attempted to estimate the formation temperatures of veins in the Lemhi Pass District. Gibson [29] estimated temperatures of 200 °C to 500 °C from monazite–xenotime and chlorite geothermometers, assuming a low pressure. Allison [41] measured temperatures of 218 °C to 330 °C for quartz-hosted inclusions and calculated salinities of 20 to 31 wt. % NaCl equivalent on Lucky Horseshoe samples. May [42] measured homogenization temperatures at four prospects in the district, recording homogenization temperatures (T_h) of quartz-hosted inclusions that varied widely but ranged from 100 °C to 392 °C with salinities of 12 to 31.1 wt. % NaCl equivalent. Fluorite-hosted inclusions homogenized at lower temperatures (76 °C to 174 °C) with

similar to slightly lower salinities. The estimated values for temperature and salinity from the fluid inclusions examined are within the moderate to moderately high temperature range for ore-forming systems, but pressures are poorly constrained.

Table 4. Sm/Nd isotopic data for single monazite crystals.

	t	[Sm]	[Nd]	^{147}Sm	^{143}Nd		*f*	Epsilon	Epsilon	$t_{DM\ (Ga)}$	$t_{DM\ (Ga)}$
Sample	**(Ga)**	**ppm**	**ppm**	**^{144}Nd**	**^{144}Nd**	**±2 s [abs]**	**Sm/Nd**	**Nd (0)**	**Nd (t)**	**1-Stage**	**2-Stage**
Monazite											
M15	0.355	42,484	293,198	0.0876	0.512312	0.000005	−0.5547	−6.36	−1.90	1.01	1.35
MB2	0.355	44,610	306,083	0.0881	0.512318	0.000007	−0.5521	−6.24	−1.81	1.01	1.34
MA3	0.355	57,837	420,601	0.0831	0.512288	0.000015	−0.5774	−6.83	−2.19	1.01	1.37

Notes: $^{143}Nd/^{144}Nd$ ratio is reported as spike-stripped and bias-corrected relative to a value of the JNdi-1 standard = 0.512110; the external reproducibility of the JNdi-1 standard over the course of the study was 0.512102 ± 3 (2 s). The uncertainty of $^{143}Nd/^{144}Nd$ is the internal standard error; uncertainty in [Sm], [Nd] and $^{147}Sm/^{144}Nd$ are estimated at ≤0.2% (2 s). Present-day εNd(0) and t_{CHUR} (Ga) calculated with $^{147}Sm/^{144}Nd_{CHUR}$ = 0.1967 and $^{143}Nd/^{144}Nd_{CHUR}$ = 0.512638; εNd(2.6) calculated at age of crystallization. 1-stage t_{DM} calculated with $^{143}Nd/^{144}Nd_{DM}$ = 0.513151, $^{147}Sm/^{144}Nd_{DM}$ = 0.2137, and the measured $^{147}Sm/^{144}Nd$ of the monazite crystal. 2-stage t_{DM} used the measured $^{147}Sm/^{144}Nd$ from present-day to 0.355 Ga (crystallization), and the $^{147}Sm/^{144}Nd$ = 0.1285 of the North American Shale Composite [35] as a proxy for the isotopic evolution of the REE source prior to monazite growth.

4. Discussion

This paper intends to highlight and document the very unusual composition of mineralization and monazites in the Lemhi Pass district, as well as the surprising geochronology results to a wider audience. It is difficult to fully evaluate the origin of these very unusual Nd-rich monazites without a more comprehensive look at the regional geology and geologic history, which is beyond the scope of this article. A critical uncertainty is simply the lack of knowledge about the subsurface geology in the district. Similarly, there is no outcrop in the area for the apparent time interval most critical to mineralization due to uplift and deformation that generated the unconformity between the Mesoproterozoic strata and overlying Eocene volcanic and sedimentary rocks. While understanding of the regional geology has advanced significantly since this project started and even more since the early prospectors first noted the Th-REE deposits, there are still many unknowns. Thus, the discussion below is rather speculative, though additional details can be found in references cited.

4.1. Comparisons to Other Monazites

Comparisons to monazites described in the literature are useful, but very few examples with such high Nd contents have been identified. Zi et al. [4] document monazite compositions from different settings, such as magmatic, metamorphic, and carbonatitic deposits. The highest Nd content analyzed or reported was about 25 wt. % Nd_2O_3, typically from authigenic rims on grains in metasedimentary rocks [4]. Figure 15 shows Lemhi Pass monazite compositions on a CaO-ThO_2-TREO ternary diagram compared with other monazites listed [4]. While the Lucky Horseshoe samples partly overlap the field of carbonatite monazite, they also plot within a broader compositional range of low-temperature metamorphic monazite. For comparison, the Roberts sample shown is from a carbonatite horizon in the Mineral Hill district (Monazite–Rutile belt in Figure 1). The Lemhi Pass monazites have a total REO content lower than in the carbonatite field, and the pattern of REE distribution is quite different. Carbonatites, such as Mountain Pass, California, or the enigmatic horizons of the Mineral Hill/Sheep Creek district of Idaho and Montana, are characterized by very high light rare earth (LREE) enrichment and a strong left-to-right

downward trend on a chondrite-normalized REE spider plot. Monazites at Mountain Pass, though affected by metasomatic (i.e., hydrothermal) processes, contain approximately 7–11 wt. % Nd_2O_3 and display the typical trend of strong La and Ce enrichments on a chondrite-normalized diagram [43]. In contrast, rocks from Lemhi Pass show a Nd and middle rare earth (MREE) enrichment or hump on a REE spider plot (Figure 9).

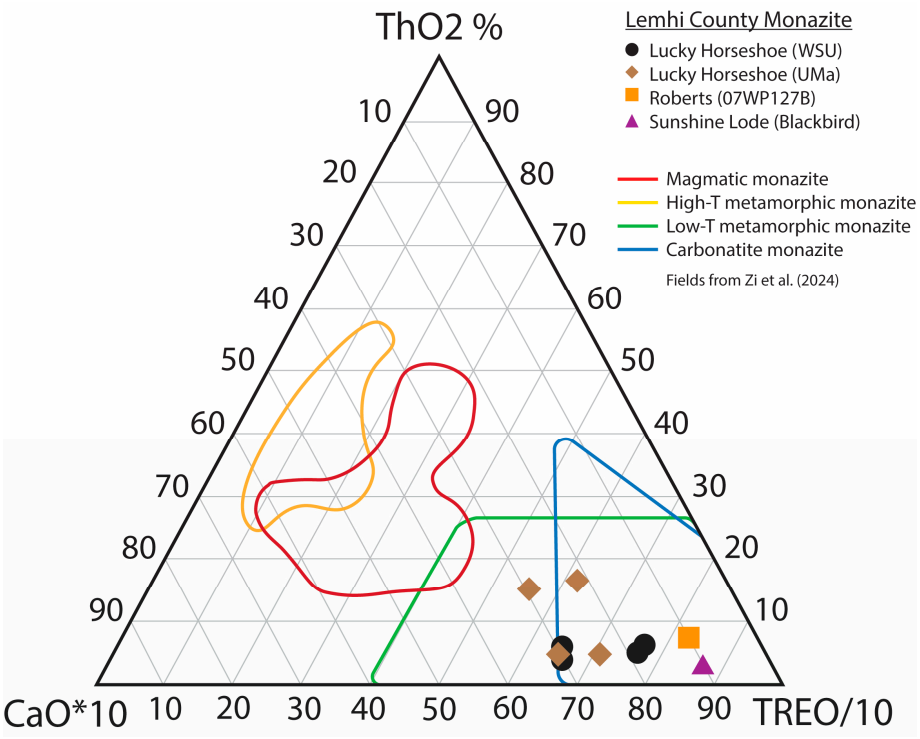


Figure 15. Lemhi Pass and two other Lemhi County monazite compositions compared to fields from classifications of Zi and others [4]. TREO = total rare earth oxide. CaO*10 refers to the % CaO multiplied by 10. TREO/10 refers to the wt. % of TREO divided by 10.

Literature descriptions of such highly enriched Nd-monazites are quite rare. In general, Nd-monazites have been described from Alpine hydrothermal veins and "grey monazite" in weakly metamorphosed metasedimentary rocks in Europe and Alaska [44,45]. Shandl and Gorton [46] studied an assortment of hydrothermal monazites and found Nd compositions ranged from about 4 to 18 weight percent Nd_2O_3. Monazite described from Pta. Glogstafel of Val Formazza in the Italian Alps is hosted in small hydrothermal fissures within aplitic to pegmatitic veins that cut micaceous gneiss; rutile and other rare earth minerals, including Ce-monazite, are also noted [44]. The crystals, described as rose-colored and prismatic, contain 30.32 wt. % Nd_2O_3 along with 6.47 wt. % Pr oxide and 8.81 wt. % Sm oxide [44].

Twardak et al. [47] described monazite-(Sm) and monazite-(Nd) with one analysis containing up to 34 wt. % Nd_2O_3 from the Blue Beryl dyke in a pegmatite system in Poland. The pegmatites are interpreted to be derived from highly fractionated partial melting of metamorphic rocks, and they feature a hybrid Be-Nb-Ta-P-Li-B geochemical signature within the pegmatites. The monazite-(Nd) crystals are only about 10 microns in size and apparently known from a single quarry.

Janots et al. [48] looked at fluid composition and evolution in a study of hydrothermal monazites from Alpine fissures in the Swiss Alps using their U-Th-Pb isotopic systematics. The crystallization is ascribed to late-stage aqueous fluids present at the end of Alpine metamorphism, and the yellow monazites are hosted in greenschist to amphibolite facies rocks. The growth zoned monazite crystals contain about 13–16.5 wt. % Nd_2O_3 as measured by EMPA, and U-Pb ages measured by SIMS analysis are quite young (13 to 16 Ma)

compared to the Lemhi Pass rocks. The Alpine monazites have very low U concentrations and very high Th/U ratios which the authors [48] ascribe to oxidizing fluids separating the more mobile U^{+6} out of the system. The Lemhi Pass monazites have very low U contents and correspondingly high Th/U ratios (Table 3). That plus the abundant hematite suggests the fluids were very oxidizing at Lemhi Pass, perhaps similar to the hydrothermal environment described for the Swiss Alpine occurrences.

A particularly intriguing example of diagenetic Nd-monazite with up to 31 wt. % Nd_2O_3 has been reported from sandstones of the Grinnell Formation of the Belt–Purcell basin, though values of <14 wt. % are more common [49,50]. Kusiak and Gonzalez-Alvarez [49] ascribed the unusual composition to the effect of a highly oxidizing fluid which can remove Ce^{+4} from the system, leaving a remnant solution rich in middle rare earth (MREE) ions. They also report that oxidizing brines are known to have affected the Belt–Purcell basin elsewhere. Moderate temperature hypersaline brines have been reported from fluid inclusions in the Idaho Copper–Cobalt belt, which is hosted in similar Belt metasedimentary rocks approximately 75 km northwest of Lemhi Pass [51].

Additional occurrences of Nd-monazite with >30 weight percent Nd oxide probably exist, but they are clearly very rare. The Nd-rich monazites at Lemhi Pass have an equal or greater percent of Nd oxide than any described in the literature, and they are also much more than a mineralogic oddity. The highly Nd-enriched monazites constitute an "ore" mineral found in veins over tens of square kilometers rather than in a single thin section.

4.2. Genesis of Lemhi Pass Nd-Monazite: Observations and Hypotheses

A comprehensive discussion of the origin of the unique Lemhi Pass deposits requires additional knowledge of the surface and subsurface geology in the district and region. A few suggestions were made previously ([14,52] and references therein), and additional observations, data and hypotheses are suggested below. The depletion of Ce in the Lemhi Pass deposits could be due to the effect of hypogene oxidation, as noted above, but a low Ce source, such as Paleozoic phosphorites or marine shales which were eroded off the top of the basement rocks is an alternative hypothesis [52]. Rare earths can be adsorbed onto iron–manganese oxyhydroxides which settle through the water column and some marine sediments and phosphorites show MREE maxima on their normalized spider diagrams [53,54].

The wide areal extent of the Nd- and MREE-enriched mineralization in multiple veins and individual deposits is notable. The Th-REE-Fe quartz veins are clearly structurally controlled and hydrothermal in origin, although the Lucky Horseshoe shear zone likely has a more complex mode of emplacement. Mineralogically, a key feature is the abundant specular hematite, intergrown with thorite as part of the primary, hypogene assemblage (Figures 7 and 8). The hematite indicates an oxidation state at or above the HMO buffer, and the district veins have minimal magnetite, further suggesting very high oxidation states during mineralization.

Only a few small intrusive bodies outcrop in the district or regionally; they were dated as early Cambrian in age (~530 Ma) and form a bimodal assemblage of syenite and mafic lamprophyres emplaced into a Neoproterozoic continental rifted margin with the early copper-bearing veins perhaps associated with the early Cambrian event [14]. Larger and slightly younger plutons (Beaverhead Pluton) of Cambrian to Ordovician age (500–485 Ma) are present to the south [55,56]. Igneous rocks, particularly alkaline intrusive complexes, can be enriched in REEs, and REE-bearing monazite and allanite are common accessory minerals in many granitic intrusives [31,57–59]. Like the Lemhi Pass syenite (Table 2), the Beaverhead pluton is not known to be particularly endowed with REEs. However, both intrusions are almost 140 million years older than the mineralization age determined in

this study. The literature examples discussed previously have in common a hydrothermal component, suggesting that high Nd-monazite is more common in hydrothermal settings (including fluid-affected pegmatites and metamorphic rocks) than in strictly igneous or carbonatite deposits, though the dataset is limited [4,44,47–49]. While hydrothermal overprints may affect and modify carbonatites, that process alone does not apparently produce the pattern or magnitude of Nd-enrichment seen at Lemhi Pass [12,43,60].

Electron microprobe dating of both monazite and thorite suggest a Devonian-Mississippian age for Th-REE mineralization with a wide halo of ages surrounding an approximate age circa 350 Ma. In the western U.S. there is considerable evidence for active tectonics at that time, such as the enigmatic Roberts Mountain thrust (Antler Orogeny) in Nevada [61–63] and early faulting of the Cambrian plutons south of Lemhi Pass [56]. It is possible that a large buried alkaline intrusive, pegmatite, or carbonatite of that age underlies the district (or has been structurally displaced or eroded from the district) but no such pluton has yet been identified. Nor does a carbonatite or peralkaline igneous source alone explain the unusual REE patterns and high Nd content of the Lemhi Pass district deposits and monazites in comparison to the literature data discussed earlier [4,31,57,58]. Future exploration work or geophysics may find new exposures of highly evolved igneous rocks or carbonatites which the large expanses of Quaternary surficial material have obscured in the district (Figure 16). However, a new genetic model may be needed to account for the widespread Nd and MREE enrichment seen at Lemhi Pass.



Figure 16. View looking northwest along the Lemhi Pass Fault zone, marked by depressed topography, with softer Cenozoic rocks faulted against Mesoproterozoic quartzites and siltites that form the higher mountains on the right side of the photo. Note the general lack of outcrop due to thick colluvial cover on the slopes.

We tentatively interpret the high Nd and MREE enriched Th-REE-Fe mineralization as a product of a dominantly hydrothermal system which sourced rare earths from a pre-existing source, possibly one already somewhat enriched in REEs. Rare earths were leached and remobilized by hydrothermal transport followed by deposition in dominantly structural traps generated during Paleozoic deformation. The fluids were apparently moderately hot, oxidized, saline, and sulfide-deficient, based on the mineral assemblages present at

Lemhi Pass. Hydrothermal mobilization of REEs, while complex, is possible [43,44,64], although a discussion of REE geochemistry is beyond the scope of this article. Perhaps the hydrothermal fluids were derived partly from regional brines that leached REEs from the large volume of Mesoproterozoic clastic metasediments and granitoids, or perhaps they leached REEs from altered early Paleozoic alkaline plutons, phosphatic shales or other unknown sources. Extensive hydrothermal circulation was apparently focused along the old rifted and extended continental margin which was a structural weakness and loci of pluton emplacement in mid-Paleozoic times [55,65]. Figure 17 is a simplified cross-section illustrating the proposed, hypothetical model.

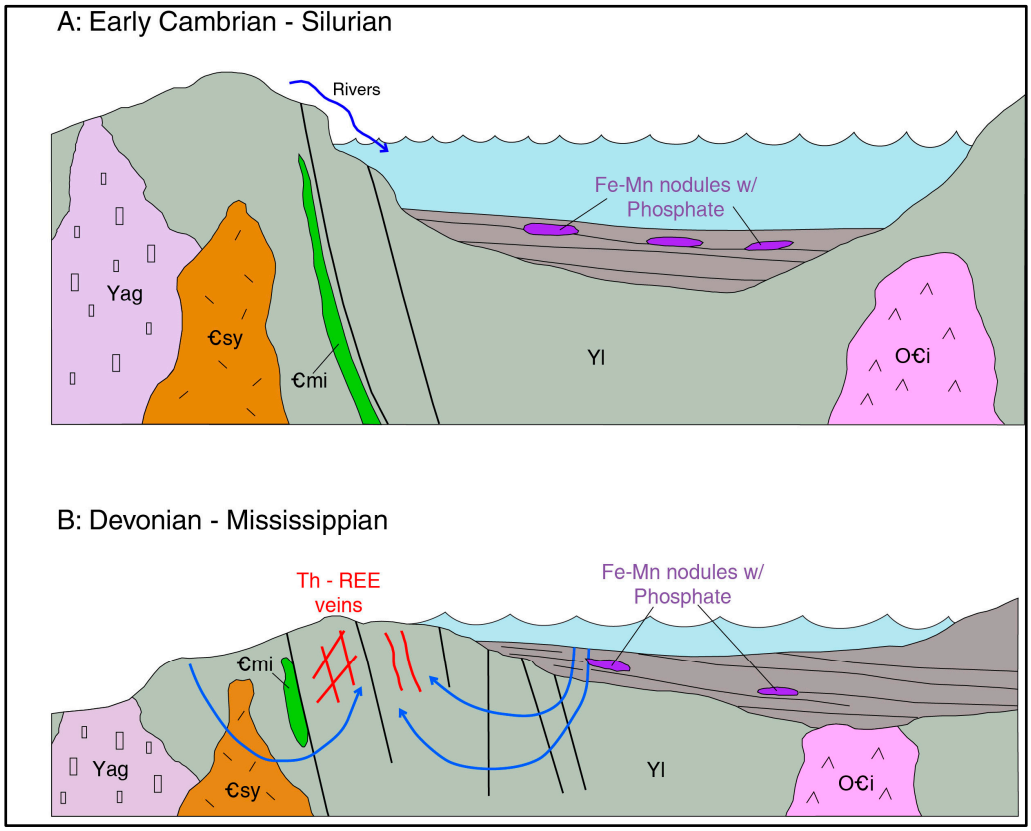


Figure 17. A cartoon rendition of a hydrothermal model for formation of Th-REE-Fe veins and deposits of the Lemhi Pass district, Idaho and Montana [52]. Potential sources of the Nd and MREE would include multiple units from Mesoproterozoic igneous and sedimentary sources, plus Paleozoic marine sediments and plutons. Yag = Mesoproterozoic augen gneiss/granite; Yl = Lemhi Group Mesoproterozoic clastic sediments; Cmi = Cambrian mafic dikes; Csy = Cambrian syenite; OCi = Ordovician–Cambrian plutons; Brownish layers = Paleozoic marine sediments with phosphate nodules indicated (purple color). Blue arrows are schematic hydrothermal fluid circulation.

The tectonics, igneous geology, and geologic evolution of Idaho during the Paleozoic are not well known. But at Lemhi Pass, that part of the stratigraphic section is represented by a large unconformity. Isotopic constraints imply that the hydrothermal fluids interacted with and largely sourced Pb and REEs from ancient Mesoproterozoic continental crust in addition to more juvenile mantle sources. The Nd and MREE enrichment may simply be due to metasomatism and metal zoning during hydrothermal fluid transport under relatively oxidizing and unusual conditions. Extreme metal zoning is characteristic of many hydrothermal or magmatic–hydrothermal ore deposits, and though not well understood quantitatively, it can reflect changes in temperature, pressure and multiple chemical changes induced by mineral precipitation during fluid–rock interaction. In this case, the more common lanthanum and cerium may have been stripped out, leaving the Th, Nd, Pr, and

MREEs enriched in the deposits. In essence, the system was a natural hydrometallurgical, chromatographic process.

The younger, volumetrically minor Cretaceous-aged rims and fracture-fillings represent a second and separate event of remobilization and recrystallization by fluids associated with the voluminous Idaho batholith and Mesozoic metamorphism and deformation which affected Idaho from about 200 Ma to 70 Ma due to tectonic convergence on the Pacific margin hundreds of kilometers to the west.

The results of this study suggest several key research questions going forward:

1. Does REE and Th mineralization in this northerly trending belt reflect a zone of metasomatized or enriched mantle and if so, how do later magmatic or hydrothermal events access this zone?
2. What is the distribution of rare earth elements in the architecture of the Mesoproterozoic rocks of the region? Only a few multi-element analyses characterize the diverse lithologies of the Lemhi sub-basin metasedimentary units or the regional suite of 1370 Ma megacrystic granites (augen gneiss) and mafic intrusive complex. Likewise, there are few analyses of the Paleozoic magmatic rocks in Lemhi County. If any of these units were indeed sources of rare earths then how much, if any, of the unusual REE fractionation could have been inherited?
3. Related to 2 above, what physiochemical processes can account for the unusual fractionation of Nd (enriched), La and Ce (depleted) relative to more typical igneous or metamorphic monazite? Has supergene (or hypogene) oxidation (common at Lemhi Pass) affected the REE distributions? Some of the most relevant variables, such as oxygen fugacity, salinity, iron content, and relatively high temperature, can be deduced from the geologic characteristics of the district, though additional alteration mapping, isotopic, geochemical, mineralogic, and fluid inclusion work is needed, as well as experimental laboratory work.

5. Conclusions

Mineralized quartz veins and biotite-bearing replacements in the Lemhi Pass district of Idaho and Montana are uniquely enriched in Nd and middle rare earth elements. Monazite is the major REE-bearing phase, and EPMA reveals the monazite from several prospects to contain approximately 35 wt. % Nd oxide, along with atypically high Pr, Eu, and Sm oxides. The hydrothermal deposits, which are present in veins scattered over tens of square kilometers, constitute Th-REE-Fe mineralization with thorite and specular hematite as major hypogene constituents. Field relations, bracketing Ar^{40}/Ar^{39} geochronology, and total Th-U-Pb EPMA chemical dating of monazite and thorite document a main period of Th-REE mineralization during the Paleozoic, with a mean age of approximately 355 Ma $\pm$ 20 Ma within a wider span (approximately 380–320 Ma) of individual age determinations. Structural reactivation along a Neoproterozoic rifted continental margin is the preferred hypothesis to have initiated large-scale hydrothermal circulation that interacted with ancient Mesoproterozoic crustal rocks and sediments, plus a small component of other, more isotopically juvenile sources such as Paleozoic plutons or marine strata or unknown mantle-derived material.

A late period of narrow, Th-rich micron-scale monazite rims record EPMA ages formed in the Cretaceous at 140–80 Ma, a time of major metamorphism and intrusion of the voluminous Idaho batholith that affected much of central Idaho.

An intersection of multiple events and rare conditions must have been needed to generate the unusual Nd-monazites and deposits at Lemhi Pass. Future work will be needed to more clearly understand the unique Lemhi Pass Th-REE-Fe mineralization.

Supplementary Materials: The following supporting information can be downloaded at: https://www.mdpi.com/article/10.3390/min15111156/s1, File S1. Summary of analytical procedure for EPMA geochronology for this study; File S2a. UMassMonaziteProbe; File S2b. WSUprobeMonazite; File S3. Sample LH06-25; File S4. Sample LH06-24B Monazite Grain Maps; File S5. MzAges; File S6. ThorAges.

Author Contributions: Conceptualization, V.S.G., M.J.J. and M.D.S.; methodology, M.J.J., M.D.S. and V.S.G.; validation, V.S.G., M.J.J. and M.D.S.; formal analysis, V.S.G., M.J.J. and M.D.S.; investigation, V.S.G., M.J.J. and M.D.S.; resources, V.S.G., M.J.J. and M.D.S.; data curation, V.S.G., M.J.J. and M.D.S.; writing original draft preparation, V.S.G.; writing—review and editing, V.S.G., M.J.J. and M.D.S.; supervision, V.S.G.; funding acquisition, V.S.G. All authors have read and agreed to the published version of the manuscript.

Funding: This research was funded principally by the U.S. Geological Survey MRERP Grant 06HQGR0170 to V.S.G. Initial field work in the Lemhi Pass district was supported by a contract to the Idaho Geological Survey from the Bureau of Land Management. Idaho Engineering and Geology, Inc., and Thorium Energy, Inc., provided minor field and analytical support.

Data Availability Statement: Data are within the article and the references therein (particularly Gillerman, 2008 [14]). Most of the data presented in this study are openly available at the Idaho Geological Survey and at USGS report page: https://www.usgs.gov/media/files/mrerp-report-06hqgr0170 (URL accessed on 26 October 2025).

Acknowledgments: We particularly thank Idaho Engineering and Geology and industry workers for field assistance and many discussions, laboratory staff at Boise State University and elsewhere, and Tony Mariano for enlightening discussions of rare earths in general. Very helpful comments by three anonymous reviewers greatly improved the manuscript. Drafting assistance from Jesslyn Starnes, Scott Gifford, Nate Hopkins, and Adam Trzinski at the Idaho Geological Survey was greatly appreciated. This article is an expanded version of a talk which was presented at the Society for Geology Applied to Mineral Deposits (SGA) 2025 Meeting in Golden, CO, USA, 3–7 August 2025.

Conflicts of Interest: The authors declare no conflicts of interest. The funders had no role in the design of the study; in the collection, analyses, or interpretation of data; in the writing of the manuscript; or in the decision to publish the results.

References

1. Anderson, A.L. Thorium Mineralization in the Lemhi Pass Area, Lemhi County, Idaho. *Econ. Geol.* **1961**, *56*, 177–197. [CrossRef]
2. Staatz, M.H.; Shaw, V.E.; Wahlberg, J.S. Occurrence and Distribution of Rare Earths in the Lemhi Pass Thorium Veins, Idaho and Montana. *Econ. Geol.* **1972**, *67*, 72–82. [CrossRef]
3. Staatz, M.H. Geology and Mineral Resources of the Lemhi Pass Thorium District, Idaho and Montana. In *U.S. Geological Survey Professional Paper 1049-A*; Geological Survey: Reston, VA, USA, 1979; p. 90.
4. Zi, J.-W.; Muhling, J.R.; Rasmussen, B. Geochemistry of Low-Temperature (<350 °C) Metamorphic and Hydrothermal Monazite. *Earth-Sci. Rev.* **2024**, *249*, 104668.
5. Anderson, A.L. Uranium, Thorium, Columbium, and Rare Earth Deposits in the Salmon Region, Lemhi County, Idaho. *Ida. Bur. Mines Geol. Pam.* **1958**, *115*, 81.
6. Sharp, W.N.; Cavender, W.S. Geology and Thorium-Bearing Deposits of the Lemhi Pass Area, Lemhi County, Idaho, and Beaverhead County, Montana. In *U.S. Geological Survey Bulletin*; US Government Printing Office: Washington, DC, USA, 1962; Volume 1126, p. 76.
7. Van Gosen, B.S.; Gillerman, V.S.; Armbrustmacher, T.J. *Thorium Deposits of the United States—Energy Resources for the Future?* U.S. Geological Survey Circular: Reston, VA, USA, 2009; Volume 1336, p. 22.
8. Gillerman, V.S. Rare Earth Elements and Other Critical Metals in Idaho. *Ida. Geol. Surv. GeoNote* **2011**, *44*, 4.
9. U.S. Geological Survey. *Mineral Commodity Summaries*; U.S. Geological Survey Circular: Reston, VA, USA, 2025; p. 212.
10. Regulation (EU) 2024/1252 of the European Parliament and of the Council of 11 April 2024, Secure and Sustainable Supply of Critical Raw Materials. Available online: http://data.europa.eu/eli/reg/2024/1252/oj (accessed on 17 July 2025).
11. Reich, M.; Simon, A.C. Critical Minerals. *Annu. Rev. Earth Planet. Sci.* **2025**, *53*, 141–168. [CrossRef]
12. Verplanck, P.; Mariano, A.N.; Mariano, A., Jr. Rare Earth Element Ore Geology of Carbonatites. In *Rare Earth and Critical Elements in Ore Deposits*; Reviews in Economic Geology 18; Society of Economic Geologists: Littleton, CO, USA, 2016; Volume 18, pp. 5–32.

13. Savage, C.N. Economic Geology of Central Idaho Blacksand Placers. *Ida. Bur. Mines Geol. Bull.* **1961**, *17*, 198.
14. Gillerman, V.S. Geochronology of Iron Oxide-Copper-Thorium-REE Mineralization in Proterozoic Rocks at Lemhi Pass, Idaho, and a Comparison to Copper-Cobalt Ores, Blackbird Mining District, Idaho. In *U.S. Geological Survey MRERP Report 06HQGR0170*; U.S. Geological Survey Circular: Reston, VA, USA, 2008; p. 148. Available online: https://www.usgs.gov/media/files/mrerp-report-06hqgr0170 (accessed on 26 October 2025).
15. Gillerman, V.S.; Schmitz, M.D.; Jercinovic, M.J.; Reed, R. Cambrian and Mississippian Magmatism Associated with Neodymium-Enriched Rare Earth and Thorium Mineralization, Lemhi Pass District, Idaho. *Geol. Soc. Am. Abstr. Programs* **2010**, *42*, 334.
16. Burmester, R.F.; Othberg, K.L.; Stanford, L.R.; Lewis, R.S.; Lonn, J.D. Geologic Map of the Agency Creek Quadrangle, Lemhi County, Idaho. In *Idaho Geological Survey DWM-182*; Idaho Geological Survey, University of Idaho: Moscow, ID, USA, 2018.
17. Burmester, R.F.; Mosolf, J.; Stanford, L.R.; Lewis, R.S.; Othberg, K.L.; Lonn, J.D. Geologic Map of the Lemhi Pass Quadrangle, Lemhi County, Idaho, and Beaverhead County, Montana. In *Idaho Geological Survey DWM-183*; Idaho Geological Survey, University of Idaho: Moscow, ID, USA, 2018.
18. Gillerman, V.S.; Otto, B.R.; Griggs, F.S. Site Inspection Report for the Abandoned and Inactive Mines in Idaho on U.S. Bureau of Land Management Property in the Lemhi Pass Area, Lemhi County, Idaho. In *Idaho Geological Survey Staff Report S-06-04*; University of Idaho: Moscow, ID, USA, 2006; p. 170.
19. Be Mezeme, E.; Cocherie, A.; Faure, M.; Legendre, O.; Rossi, P. Electron Microprobe Monazite Geochronology of Magmatic Events: Examples from Variscan Migmatites and Granitoids, Massif Central, France. *Lithos* **2006**, *87*, 276–288. [CrossRef]
20. Rasmussen, B.; Fletcher, I.R.; Muhling, J.R. In Situ U-Pb Dating and Element Mapping of Three Generations of Monazite: Unravelling Cryptic Tectonothermal Events in Low-Grade Terranes. *Geochem. Cosmochim. Acta* **2007**, *71*, 670–690. [CrossRef]
21. Williams, M.L.; Jercinovic, M.J.; Hetherington, C.J. Microprobe Monazite Geochronology: Understanding Geologic Processes through Integration of Composition and Chronology. *Annu. Rev. Earth Planet. Sci.* **2007**, *37*, 137–175. [CrossRef]
22. Williams, M.L.; Jercinovic, M.J.; Mahan, K.H.; Dumond, G. Electron Microprobe Petrochronology. *Mineral. Soc. Am. Rev. Mineral. Geochem.* **2017**, *83*, 153–182. [CrossRef]
23. Jercinovic, M.J.; Williams, M.L.; Lane, E.D. In-Situ Trace Element Analysis of Monazite and Other Fine-Grained Accessory Minerals by EPMA. *Chem. Geol.* **2008**, *254*, 197–215. [CrossRef]
24. Cottle, J.M. In Situ U-Th/Pb Geochronology of (Urano)Thorite. *Am. Mineral.* **2014**, *99*, 1985–1995. [CrossRef]
25. Jercinovic, M.J.; Williams, M.L. Analytical Perils (and Progress) in Electron Microprobe Trace Element Analysis Applied to Geochronology: Background Acquisition, Interferences, and Beam Irradiation Effects. *Am. Mineral.* **2005**, *90*, 526–546. [CrossRef]
26. Lumpkin, G.R.; Chakoumakos, B.C. Chemistry and Radiation Effects of Thorite-Group Minerals from the Harding Pegmatite, Taos County, New Mexico. *Am. Mineral.* **1988**, *73*, 1405–1419.
27. Williams, M.L.; Jercinovic, M.J.; Goncalves, P.; Mahan, K. Format and Philosophy for Collecting, Compiling, and Reporting Microprobe Monazite Ages. *Chem. Geol.* **2006**, *225*, 1–15. [CrossRef]
28. Ancey, M.; Bastenaire, F.; Tixier, R. Applications of Statistical Methods in Microanalysis. In *Microanalysis and Scanning Electron Microscopy*; Les Editions de Physique: Paris, France, 1978; pp. 319–343.
29. Gibson, P.E. Origin of the Lemhi Pass REE-Th Deposits, Idaho/Montana: Petrology, Mineralogy, Paragenesis, Whole Rock Chemistry and Isotope Evidence. Master's Thesis, University of Idaho, Moscow, ID, USA, 1998; p. 320.
30. Schipper, W.B. The Tendoy Copper Queen Mine. Master's Thesis, University of Idaho, Moscow, ID, USA, 1955.
31. Long, K.R.; Van Gosen, B.S.; Foley, N.K.; Cordier, D. The Principal Rare Earth Elements Deposits of the United States—A Summary of Domestic Deposits and a Global Perspective. In *U.S. Geological Survey Scientific Investigations Report 2010-5220*; Springer: Dordrecht, The Netherlands, 2010; p. 96.
32. Gibson, P.; Wood, S.A. Geochemistry and Mineralogy of the Lemhi Pass Th-REE Deposits. In *Mineral Deposits: Research and Exploration*; Fourth Biennial SGA Meeting; Balkema: Rotterdam, The Netherlands, 1997; pp. 945–948.
33. Idaho Strategic Resources Idaho Strategic's Lemhi Trenching Returns up to 5% Total Rare Earths—Including Magnet REE Concentrations in Excess of 70%. Available online: https://idahostrategic.com/idaho-strategics-lemhi-trenching-returns-up-to-5-total-rare-earths-including-magnet-ree-concentrations-in-excess-of-70/ (accessed on 19 July 2025).
34. Murchland, M.; Williams, T.J.; Lewis, R.S.; Gillerman, V.S.; Steven, C. Investigating Carbonatites and Rare Earth Mineralization in Lemhi County, Idaho. *Geol. Soc. Am. Abstr. Programs* **2023**, *55*, 393780.
35. Taylor, S.R.; McLennan, S.M. *The Continental Crust: Its Composition and Evolution*; Blackwell Scientific: Oxford, UK, 1985; p. 312.
36. Evans, K.V.; Green, G.N. Geologic Map of the Salmon National Forest and Vicinity, East-Central Idaho. In *U.S. Geological Survey Map I-2765*; U.S. Geological Survey: Reston, VA, USA, 2003.
37. Gillerman, V.S.; Schmitz, M.D.; Jercinovic, M.J. REE-Th Deposits of the Lemhi Pass Region, Northern Rocky Mountains—Paleozoic Magmas and Hydrothermal Activity along a Continental Margin. *Geol. Soc. Am. Abstr. Programs* **2013**, *45*, 41.
38. Gillerman, V.S.; Schmitz, M.D.; Jercinovic, M.J. Copper and REE-Th Metallogeny in Lemhi County, Idaho: Magmatism and Repeated Hydrothermal Activity along a Paleozoic Continental Margin. In *Proceedings of the Society of Economic Geologists 2013 Conference Abstracts and e-Posters*; Society of Economic Geologists: Whistler, BC, Canada, 2013.

39. Frost, C.D.; Winston, D. Nd Isotope Systematics of Coarse- and Fine-Grained Sediments: Examples from the Middle Proterozoic Belt-Purcell Supergroup. *J. Geol.* **1987**, *95*, 309–327. [CrossRef]
40. Gaschnig, R.M.; Vervoort, J.D.; Lewis, R.S.; Tikoff, B. Isotopic Evolution of the Idaho Batholith and Challis Intrusive Province, Northern US Cordillera. *J. Petrol.* **2011**, *52*, 2397–2429. [CrossRef]
41. Allison, G.K. Fluid Inclusion Evidence for the Temperature and Composition of Ore Fluids in the Lemhi Pass and Diamond Creek REE-Th Districts, Idaho-Montana. Master's Thesis, University of Missouri-Columbia, Columbia, MO, USA, 2019; p. 58.
42. May, R.A. Geochemical Evidence for the Origin of Th-REE Mineralization in the Lemhi Pass District, Idaho/Montana. Master's Thesis, University of Missouri-Columbia, Columbia, MO, USA, 2024; p. 84.
43. Benson, E.K.; Watts, K.E. Apatite and Monazite Geochemistry Record Magmatic and Metasomatic Processes in Rare Earth Element Mineralization at Mountain Pass, California. *Econ. Geol.* **2024**, *119*, 1611–1642. [CrossRef]
44. Graeser, S.; Schwander, H. Gasparite-(Ce) and Monazite-(Nd): Two New Minerals to the Monazite Group from the Alps. *Schweiz. Mineral. Petrogr. Mitteilungen* **1987**, *67*, 101–113.
45. Laval, M. Properties and Geology of Grey Monazite: A Possible New Resource of REE. In *Special Volume 50*; Canadian Institute of Mining: Montreal, QC, Canada, 1998; Volume 50, pp. 193–204.
46. Schandl, E.S.; Gorton, M.P. A Textural and Geochemical Guide to the Identification of Hydrothermal Monazite: Criteria for Selection of Samples for Dating Epigenetic Hydrothermal Ore Deposits. *Econ. Geol.* **2004**, *99*, 1027–1035. [CrossRef]
47. Twardak, D.; Pieczka, A.; Kotowski, J.; Nejbert, K. Mineral Chemistry and Genesis of Monazite-(Sm) and Monazite-(Nd) from the Blue Beryl Dyke of the Julianna Pegmatite System at Pilawa Gorna, Lower Silesia, Poland. *Mineral. Mag.* **2023**, *87*, 575–581. [CrossRef]
48. Janots, E.; Berger, A.; Gnos, E.; Whitehouse, M.; Lewin, E.; Pettke, T. Constraints on Fluid Evolution during Metamorphism from U-Th-Pb Systematics in Alpine Hydrothermal Monazite. *Chem. Geol.* **2012**, *326*, 61–71. [CrossRef]
49. Kusiak, M.A.; Gonzalez-Alvarez, I. Nd-Monazite Occurrence in North America: Mesoproterozoic Siliciclastic Rocks of the Belt-Purcell Supergroup. *Proc. Geochem. Cosmochim. Acta* **2006**, *70*, A338. [CrossRef]
50. Gonzalez-Alvarez, I.; Kusiak, M.A.; Kerrich, R. A Trace Element and Chemical Th-U Total Pb Dating Study in the Lower Belt-Purcell Supergroup, Western North America: Provenance and Diagenetic Implications. *Chem. Geol.* **2006**, *230*, 140–160. [CrossRef]
51. Landis, G.P.; Hofstra, A.H. Ore Genesis Constraints on the Idaho Cobalt Belt from Fluid Inclusion Gas, Noble Gas Isotope, and Ion Ratio Analyses. *Econ. Geol.* **2012**, *107*, 1189–1205. [CrossRef]
52. Gillerman, V.S.; Schmitz, M.D.; Jercinovic, M.J. Nd-Enriched Lemhi Pass REE-Th District, Idaho-Montana: A Link between Crustal Hydrothermal Circulation and Devonian-Carboniferous Marine Environments? *Geol. Soc. Am. Abstr. Programs* **2021**, *53*, 365142.
53. Emsbo, E.; McLaughlin, P.I.; du Bray, E.A.; Anderson, E.; Vandenbrouchke, T.; Zielinski, R.A. Rare Earth Elements in Sedimentary Phosphorite Deposits: A Global Assessment. In *Rare Earth and Critical Elements in Ore Deposits*; Reviews in Economic Geology 18; Society of Economic Geologists: Littleton, CO, USA, 2016; Volume 18, pp. 101–113.
54. Emsbo, P.; McLaughlin, P.I.; Breit, G.N.; du Bray, E.A.; Koenig, A.E. Rare Earth Elements in Sedimentary Phosphate Deposits: Solution to the Global REE Crisis? *Gondwana Res.* **2015**, *27*, 776–785. [CrossRef]
55. Lund, K.; Aleinikoff, J.N.; Evans, K.V.; Dubray, E.A.; Dewitt, E.H.; Unruh, D.M. SHRIMP U-Pb Dating of Recurrent Cryogenian and Late Cambrian–Early Ordovician Alkalic Magmatism in Central Idaho: Implications for Rodinian Rift Tectonics. *GSA Bull.* **2010**, *122*, 430–453. [CrossRef]
56. Parker, S.D.; Pearson, D.M. Field Guide to Carbonate Mylonites and Reactivated Basement Faults of the Leadore Area. *Northwest Geol.* **2023**, *52*, 197–210.
57. Dostal, J. Rare Metal Deposits Associated with Alkaline/Peralkaline Igneous Rocks. In *Rare Earth and Critical Elements in Ore Deposits*; Reviews in Economic Geology 18; Society of Economic Geologists: Littleton, CO, USA, 2016; Volume 18, pp. 33–52.
58. Chakhmouradian, A.R.; Zaitsev, A.N. Rare Earth Mineralization in Igneous Rocks: Sources and Processes. *Elements* **2012**, *8*, 347–353. [CrossRef]
59. Mariano, A.N.; Mariano, A., Jr. Rare Earth Mining and Exploration in North America. *Elements* **2012**, *8*, 369–376. [CrossRef]
60. Nadeau, O.; Stevenson, R.; Jébrak, M. Evolution of Montviel Alkaline–Carbonatite Complex by Coupled Fractional Crystallization, Fluid Mixing and Metasomatism—Part I: Petrography and Geochemistry of Metasomatic Aegirine–Augite and Biotite: Implications for REE–Nb Mineralization. *Ore Geol. Rev.* **2016**, *72*, 1143–1162. [CrossRef]
61. Cashman, P.H.; Sturmer, D.M. The Antler Orogeny Reconsidered and Implications for Late Paleozoic Tectonics of Western Laurentia. *Geology* **2023**, *51*, 543–548. [CrossRef]
62. Trexler, J.H., Jr.; Cashman, P.H.; Cole, J.C.; Snyder, W.S.; Tosdal, R.M.; Davydov, V.I. Widespread Effects of Middle Mississippian Deformation in the Great Basin of Western North America. *GSA Bull.* **2003**, *115*, 1278–1288. [CrossRef]
63. Trexler, J.H., Jr.; Cashman, P.H.; Snyder, W.S.; Davydov, V.I. Late Paleozoic Tectonism in Nevada: Timing, Kinematics, and Tectonic Significance. *GSA Bull.* **2004**, *116*, 525–538. [CrossRef]

64. Williams-Jones, A.E.; Migdisov, A.A.; Samson, I.M. Hydrothermal Mobilisation of the Rare Earth Elements—A Tale of "Ceria" and "Yttria". *Elements* **2012**, *8*, 355–360. [CrossRef]
65. Lund, K. Geometry of the Neoproterozoic and Paleozoic Rift Margin of Western Laurentia: Implications for Mineral Deposit Settings. *Geosphere* **2008**, *4*, 429–444. [CrossRef]

Disclaimer/Publisher's Note: The statements, opinions and data contained in all publications are solely those of the individual author(s) and contributor(s) and not of MDPI and/or the editor(s). MDPI and/or the editor(s) disclaim responsibility for any injury to people or property resulting from any ideas, methods, instructions or products referred to in the content.